





34 comparable between AMX (60%) and TRO (54%), however only half of the observed NPF  
35 events at both sites were observed concurrently. The smaller mode diameter at AMX than at  
36 TRO indicates that NPF was initiated near AMX. This is supported by peaks in ion and particle  
37 concentrations that were first observed at AMX and followed by a 1-2 hour delay at TRO. This  
38 indicates that transported precursor vapour-laden air from lower-altitudes, likely driven by  
39 vertical mixing or up-valley winds, significantly contributes to secondary aerosol formation at  
40 the mountain site. Airmass history analysis further revealed that significant trajectories had  
41 been in contact with the PBL before reaching TRO, underscoring the influence of vertical  
42 dynamical mixing on NPF processes. The TRO site is within the PBL for about 25% of days  
43 during late winter and early spring, increasing to >80% for the rest of the year, which supports  
44 our findings. Our results highlight the significant impact of secondary aerosol production in  
45 the evolving PBL on higher-altitude environments, though the vertical extent of nucleation  
46 processes remains unclear. Understanding these processes is crucial for climate models, as the  
47 PBL drives the exchange of energy, moisture and atmospheric constituents, including aerosols,  
48 with the atmosphere above.

49

## 50 **1. Introduction**

51 Atmospheric new particle formation (NPF) events involve the formation of molecular clusters,  
52 via gas-to-particle conversion, from precursor vapours such as sulfuric acid, ammonia, amines,  
53 oxidation products of volatile organic compounds, and other trace gases that can form low-  
54 volatility complexes, and subsequent growth of these small clusters to larger particles  
55 (Kulmala, 2003; Zhang et al., 2004). Globally, NPF is the largest source of aerosol numbers in  
56 the atmosphere (Kerminen et al., 2012; Wang and Penner, 2009). These newly formed particles  
57 can reach CCN sizes (particle diameter of 50-100 nm and larger) by coagulation and  
58 condensation of additional vapours (Kerminen et al., 2018; Sebastian et al., 2022; Pierce and  
59 Adams, 2009; Westervelt et al., 2013; Williamson et al., 2019). Global modelling simulations  
60 showed that NPF events produce half of the present-day global CCN number (Merikanto et al.,  
61 2009; Spracklen et al., 2008; Westervelt et al., 2014; Yu and Luo, 2009), with an estimated  
62 uncertainty range from 38 to 66% (Gordon et al., 2017). The uncertainty in CCN production in  
63 the global climate model itself stems partly from the uncertainty in particle formation and  
64 growth (IPCC, 2023). Additionally, human exposure to inhalable fine particles, from both  
65 primary and secondary sources, has serious health risks that can lead to premature death  
66 (Lelieveld et al., 2019).

67



68 To date, there are a scanty number of studies investigating characteristics of NPF events over  
69 Cyprus (Baalbaki et al., 2021; Brilke et al., 2020; Debevec et al., 2018; Gong et al., 2019) and  
70 overall the limited number of studies over the EMME region (Aktypis et al., 2023; Aktypis et  
71 al., 2024; Dinoi et al., 2023; Hakala et al., 2019; Hussein et al., 2020; Hakala et al., 2023;  
72 Pikridas et al., 2012; Kalkavouras et al., 2019; Kalivitis et al., 2019; Kalkavouras et al., 2020;  
73 Kalkavouras et al., 2021; Manninen et al., 2010). The EMME region is characterised by diverse  
74 air masses originating from continental, maritime, and desert areas, which affect the  
75 atmospheric composition and climate in the area (Bimenyimana et al., 2023; Vrekoussis et al.,  
76 2022; Zittis et al., 2022). While NPF events have been frequently observed in western Saudi  
77 Arabia without any clear seasonal pattern (Hakala et al., 2019), Hussein et al. (2020) observed  
78 the highest NPF event frequency during summer in Amman, Jordan. In contrast, NPF events  
79 were frequently observed during spring and autumn in the eastern Mediterranean (Baalbaki et  
80 al., 2021; Kalivitis et al., 2019). The frequent occurrence of NPF events in the eastern  
81 Mediterranean has been linked to various factors, such as solar radiation/temperature, terrestrial  
82 biogenic activity, higher sulfuric acid (H<sub>2</sub>SO<sub>4</sub>) concentrations, high-dust episodes, and/or air  
83 mass history, but it is still not completely clear what drives the frequent occurrence of NPF  
84 events over this region (Baalbaki et al., 2021). A previous study showed that NPF events  
85 occurred on 58% of days annually at a lower-altitude site (AMX) (Baalbaki et al., 2021), which  
86 is the highest reported frequency after South Africa (86%) (Hirsikko et al., 2012) and Saudi  
87 Arabia (73%) (Hakala et al., 2019). In contrast, NPF events occurred only on 12% of days  
88 during summer at a higher-altitude mountain site (Helmos mountain at 2314 m a.m.s.l.) in  
89 Greece (Aktypis et al., 2024). Previous studies have shown that NPF events at higher-altitude  
90 locations occur under the influence of up-valley winds, which channel precursor gases to higher  
91 altitudes, typically when the boundary layer extends above the site's altitude (Bianchi et al.,  
92 2016; Tröstl et al., 2016a; Sebastian et al., 2021), and NPF events were observed even at higher  
93 vapour condensation sink compared to non-events (Sellegri et al., 2019). On the contrary,  
94 Boulon et al. (2011) showed that NPF events were observed more frequently in the free  
95 troposphere (43.5% of the total observation days at the Puy de Dôme station, 1465 m a.m.s.l.)  
96 than within the PBL lower-altitude (2.5% of the total observation days at the Opme station,  
97 660 m a.m.s.l.) in Central France.

98

99 Up to which altitude NPF events take place, and where they are initiated is still unclear.  
100 Although NPF events have been extensively studied worldwide (Nieminen et al., 2014;  
101 Kerminen et al., 2018; Nieminen et al., 2018; Lee et al., 2019; Kulmala et al., 2004), limited



102 studies have been focused on vertical extent of NPF processes (Wehner et al., 2010; Stratmann  
103 et al., 2003; Minguillón et al., 2015). Minguillón et al. (2015) demonstrated that intense NPF  
104 events in Barcelona primarily occur at a surface level around midday, coinciding with high  
105 insolation and pollution dilution, whereas early-morning NPF events are constrained to higher  
106 altitudes due to the inhibition of these events by high surface-level condensation sink (CS).  
107 Carnerero et al. (2018) demonstrated that ultrafine particles are formed exclusively inside the  
108 mixed layer, and as the mixed layer grows, ultrafine particles are detected at higher levels  
109 within PBL, and Wehner et al. (2010) observed well-mixed ultrafine particles (5-10 nm)  
110 throughout the PBL. Furthermore, O'Donnell et al. (2023) utilised a one-dimensional coupled  
111 column model (SOM-TOMAS, Statistical Oxidation Model of organic chemistry and Two  
112 Moment Aerosol Sectional microphysics model) to demonstrate that enhanced NPF rates in the  
113 upper mixed layer are strongly influenced by temperature, vertical mixing, and gas-phase  
114 precursor concentrations.

115

116 In this work, we used semi-continuous concurrent measurements of ion and particle size  
117 distributions for the year 2022 from a lower-altitude rural background site (AMX) and a higher-  
118 latitude mountain background site (TRO) in Cyprus with a 1287 m difference in altitude in 20  
119 km distance between the observational sites. The main aim is to examine the effect of PBL  
120 evolution on NPF events at a background mountain site in Cyprus.

121

## 122 **2. Materials and methods**

### 123 **2.1 Measurement Sites**

124 AMX and TRO are sites of the Cyprus Atmospheric Observatory (CAO) network, operated by  
125 the Climate and Atmosphere Research Center (CARE-C) of the Cyprus Institute. The AMX  
126 site (35.038692° N, 33.057850° E) is located at 532 m a.m.s.l. between two villages, Agia  
127 Marina Xyliatou and Xyliatos, at the foothills of the Troodos mountain range in the central  
128 Republic of Cyprus. The AMX site is located about 1.5 km South of Agia Marina Xyliatou and  
129 about 2.2 km Northeast of Xyliatos. The AMX site hosts instruments affiliated with several  
130 research infrastructures such as the cooperative program for monitoring and evaluation of the  
131 long-range transmission of air pollutants in Europe (referred to as the European Monitoring  
132 and Evaluation Programme, EMEP), the air quality network of Cyprus operated by the  
133 Department of Labour Inspection (DLI), regional Global Atmospheric Watch (GAW) program  
134 of the World Meteorological Organization (WMO), the Aerosols, Clouds and Trace Gases  
135 Research Infrastructure (ACTRIS) aerosol in situ network, e-Profile (part of EUMETNET),

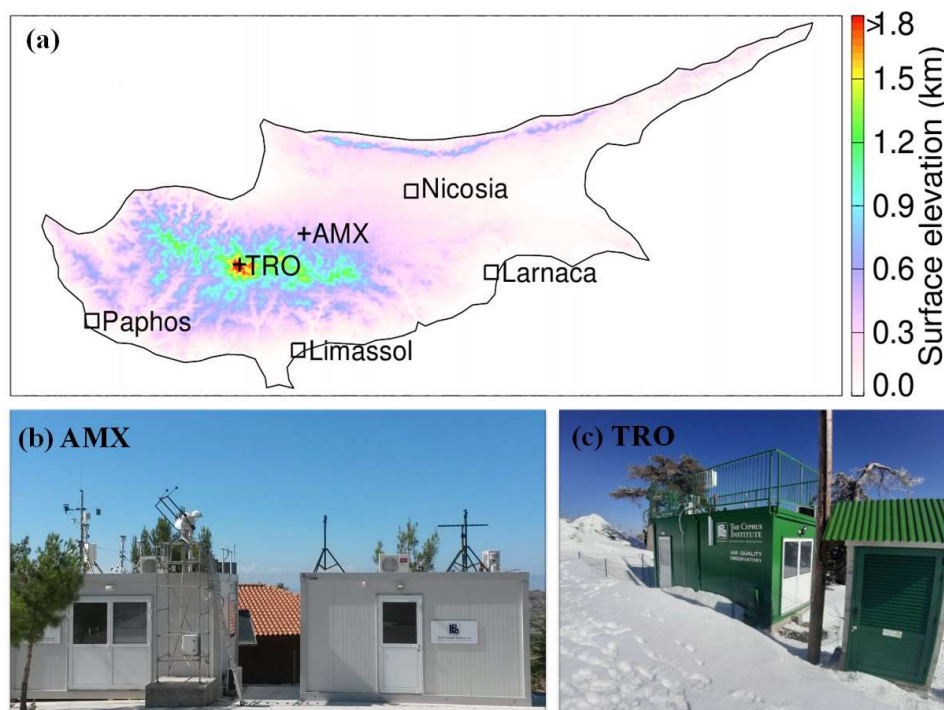


136 and NASA's AERosol RObotic NETwork (AERONET). Anthropogenic emissions in the  
137 vicinity of the AMX site are minimal and the major cities are located at about 35 km (Nicosia)  
138 to the Northeast and about 50 km (Larnaca) to the Southeast.

139

140 The TRO site (34.9430333° N, 32.8654729 E) is located at 1819 m a.m.s.l., close to Mount  
141 Olympus (the highest peak of Cyprus, 1952 m a.m.s.l.) and experiences free tropospheric  
142 conditions, primarily during winter. TRO site may also experience light to moderate snowfall  
143 during winter, usually in January and February, and it is in cloud sporadically. The site is  
144 considered a background higher-altitude mountain location as it has little or no influence from  
145 local anthropogenic activities, except occasional camping or campfire activities in the vicinity  
146 and the staging post for helicopter operations. Small villages such as Prodromos, Palaiomylos,  
147 and Agios Dimitrios are located to the West of the TRO site, while the Troodos village is  
148 located to the Southeast within a 5 km distance. It is located centrally with respect to the major  
149 cities: Limassol, about 36 km to the South, Paphos, 42 km to the Southwest, Nicosia, 50 km to  
150 the Northeast, and Larnaca, 70 km to the Southeast. Figure 1 shows the surface elevation map  
151 of Cyprus depicting the locations of AMX and TRO sites and pictures of the AMX and TRO  
152 site premises.

153



154

155 **Figure 1.** (a) Surface elevation map of Cyprus, including the location of AMX and TRO  
156 observational sites and the major cities. Elevation data is obtained from the U.S. Geological  
157 Survey global digital elevation model (DEM) with a horizontal grid spacing of 30 arc seconds  
158 (approximately 1 km (GTOPO30)). (b) and (c) show AMX and TRO site premises pictures,  
159 respectively.

160

## 161 2.2 Instrumentation

### 162 2.2.1 Neutral Cluster and Air Ion Spectrometer (NAIS)

163 The ion and total particle number size distributions were measured using the NAIS (Airel Ltd.  
164 Estonia) at both measurement sites to detect and characterise NPF events. The NAIS measures  
165 the number size distribution of ions and naturally charged particles in the diameter range of 0.8  
166 – 42 nm for NTP conditions (mobility range:  $3.162 - 0.0013 \text{ cm}^2 \text{ V}^{-1} \text{ s}^{-1}$ ) (Mäkelä et al., 1996),  
167 simultaneously in both positive and negative polarity (Manninen et al., 2016; Mirme and  
168 Mirme, 2013). Additionally, the NAIS can measure the total particle size distribution by using  
169 corona charging. Briefly, the NAIS has two parallel cylindrical differential mobility analysers  
170 (DMAs): one classifies positively charged ions, and the other classifies negatively charged



171 ions. The air is sampled at a flow rate of  $54 \text{ L min}^{-1}$ , with a sampling tube inner diameter of 30  
172 mm and a length of 65 cm. Subsequently, the airflow is divided equally for each polarity before  
173 entering the preconditioning unit. Here, depending on the operational mode, the aerosol  
174 samples either pass through without modification (ion mode), or they are charged to the same  
175 polarity of the analysers (particle mode) or they are charged to the opposite polarity of the  
176 analyser (offset mode). The air sample then reaches the analysers, where it is size-classified in  
177 an electrical field and detected by electrometers. The total particle concentration below  $\sim 2 \text{ nm}$   
178 cannot be detected due to the ions produced by the corona charger itself, and therefore  
179 discarded in the data analyses. The NAIS SPECTOPS software with an instrument-specific  
180 algorithm was used to invert the raw counts into a size distribution. The inverted data was  
181 subsequently corrected for line losses using the Gormley and Kennedy equation for inlet line  
182 losses for laminar flow (Gormley and Kennedy, 1949). Note that data gaps in NAIS  
183 measurements are present due to the instrument's unavailability or malfunction (Fig. S1).

184

### 185 *2.2.2 Ceilometer CL51*

186 The Vaisala Ceilometer CL51 is part of the E-PROFILE network, operational since 2021  
187 which coordinates the measurements of vertical profiles of wind, aerosol, and clouds from  
188 radars, lidars, and ceilometers from a network of locations across Europe and provides the data  
189 to the end users. The Vaisala Ceilometer CL51 utilises an eye-safe indium gallium arsenic  
190 (InGAs) diode-laser lidar technology, emitting 110 ns-long pulses with a wavelength of  
191  $910 \pm 10 \text{ nm}$  and a repetition rate of 6.5 kHz in a vertical or near-vertical direction (Münkel and  
192 Roininen, 2010). The CL51 can measure aerosols and clouds from above the overlap region  
193  $\sim 300 \text{ m}$  up to 15 km nominally, with a vertical resolution of 10 m. The backscatter profile is  
194 used to identify up to three aerosol-layer heights using the gradient method in the  
195 postprocessing software provided by the manufacturer (BL-VIEW), which includes an  
196 automated mixing height detection algorithm described by Emeis et al. (2007). The VAISALA  
197 BL-VIEW software features a “cloud and precipitation filter” known as the enhanced gradient  
198 method (Münkel and Roininen, 2010), which filters out high backscatter signals from clouds  
199 and precipitation before applying the gradient method. BL-View's calculation is based on the  
200 combined gradient and idealised backscatter methods that enable reliable automatic estimation  
201 of the PBL height (PBLH) at a temporal resolution of 16 seconds and a vertical resolution of  
202 10 m. Here, we used Level 3 boundary layer height data with a quality control index of “good”  
203 only.

204



### 205 **2.2.3 Ancillary measurements**

206 We used aerosol optical depth (AOD) and angstrom exponent (AE) data from the AERONET  
207 sunphotometers at both AMX and TRO sites. Trace gas concentrations, such as sulfur dioxide  
208 (SO<sub>2</sub>) and ozone (O<sub>3</sub>), and the meteorological parameters (temperature, relative humidity, solar  
209 radiation, wind speed, and wind direction) at AMX station were taken from the air quality  
210 network of Cyprus operated by the DLI. At the TRO site, TELEDYNE gas analysers for SO<sub>2</sub>  
211 (Model T100U) and O<sub>3</sub> (Model T400) were deployed and meteorological parameters were  
212 obtained from the Department of Meteorology automatic weather station, located about 3.3 km  
213 south of the measurement site. Note that all data is reported in Universal Time Coordinated  
214 (UTC). Local time in Cyprus is UTC+2 from late October to late March (Eastern European  
215 Time) and UTC+3 from late March to late October during daylight saving time (Eastern  
216 European Summer Time).

217

### 218 **2.3 Tracers used to investigate PBL evolution**

219 We used two approaches to examine the influence of PBL evolution on the occurrence of NPF  
220 events at the mountain background site, TRO. AMX is assumed to be in the PBL at all times.  
221 First, the water vapour mixing ratio (WVMR) at TRO was used to distinguish between free  
222 tropospheric (FT) and PBL air. A threshold WVMR value of 5.25 g/kg (denotes the 30th  
223 percentile value of WVMR at the AMX site) was used, with WVMR values below 5.25 g/kg  
224 indicating FT air (Zha et al., 2023). WVMR was calculated as follows:

225

$$226 \quad WVMR = B \times \frac{e}{p - e} \quad \text{---(1)}$$

227

228 where B is a constant (621.9907 g kg<sup>-1</sup>, molecular weight ratio of water to dry air), e and p are  
229 the water vapour pressure and the atmospheric pressure, respectively. e was calculated using  
230 ambient temperature, RH, and pressure (Buck, 1981).

231

232 Secondly, the Vaisala ceilometer estimated PBLH from the AMX site was used to examine the  
233 PBL evolution up to the altitude of the TRO site. The PBLH estimation algorithm might be  
234 influenced by boundary layer stability, near-surface or elevated aerosol layers, moving cloud  
235 systems in the vicinity of the measurement site, and surface type (Zhang et al., 2022). ERA5  
236 PBLH is realistically simulated by the bulk Richardson number method (Hersbach et al., 2020).  
237 Zhang et al. (2022) also showed that ceilometer estimated PBLH generally compares well with





238 the bulk Richardson number method under stable conditions. Therefore, we apply a robust data  
239 filtering technique to remove under or over-estimated PBLH data values in conjunction with  
240 ERA5 PBLH data (Hersbach et al., 2023), the latest version of ECMWF reanalysis, which is  
241 available on a  $1440 \times 721$  longitude and latitude grid, with a spatial resolution of  $0.25^\circ \times 0.25^\circ$   
242 and a temporal resolution of 1 hour. First, we remove ceilometer estimated PBLH which is  
243 lower or greater than three standard deviations of PBLH for a given day. Second, we used  
244 ERA-5 PBLH to match the diurnal pattern and considered only those days when the correlation  
245 coefficient between ERA5 and Ceilometer PBLH was greater than 0.5 at a statistical  
246 significance level of 95%. After applying these constraints, we retained 5688 hourly data points  
247 from a total of 7248 valid hourly data points, thereby ensuring that only the most reliable data  
248 were included in the PBLH analysis.

249

#### 250 **2.4 Event classification**

251 The traditional ways to classify the given day into different types of NPF events (Dal Maso et  
252 al., 2005; Hirsikko et al., 2007; Kulmala et al., 2012; Manninen et al., 2010) are mainly based  
253 on the visual appearance of a contour plot of particle number size distributions. A day with the  
254 appearance of a new particle mode followed by its growth is identified as an NPF event day  
255 and such events occur over a spatial scale of a few 100's kilometres and a temporal scale of 1-  
256 2 days and are thus referred to as regional NPF events. The downside of these methods is a  
257 large fraction of unclear days, which could be caused by more local NPF events, changes in air  
258 masses, or varying weather conditions. Such unclear events can also be further classified into  
259 different sub-classes (nucleation-mode peak, Aitken-mode, and tail), but it requires additional  
260 information on trace gases and aerosol characteristics (Kanawade et al., 2014; Buenrostro  
261 Mazon et al., 2009). However, the data analysis becomes more complex when these unclear  
262 days form a large fraction of all the days. In addition, these methods omit potentially low-  
263 intensity NPF events such as local or short-lived NPF events (Kulmala et al., 2024). Here, we  
264 used the traditional methodology for classifying a given day into NPF event, non-event and  
265 unclear. Given the asynchronous data gaps in NAIS measurements at both sites, we introduced  
266 an additional category labelled 'nodata,' which must be considered when comparing the  
267 frequency of occurrence of different event types. Nodata days include the unavailability of the  
268 instrument, maintenance (mainly the cleaning of the instrument during the summer and dust  
269 episodes), troubleshooting of the instrument, and infrequent power cuts at the measurement  
270 site. We present the frequency of occurrence for all these event types and utilise only NPF  
271 events for data analysis in this work.



272 **2.5 Air mass history analysis**

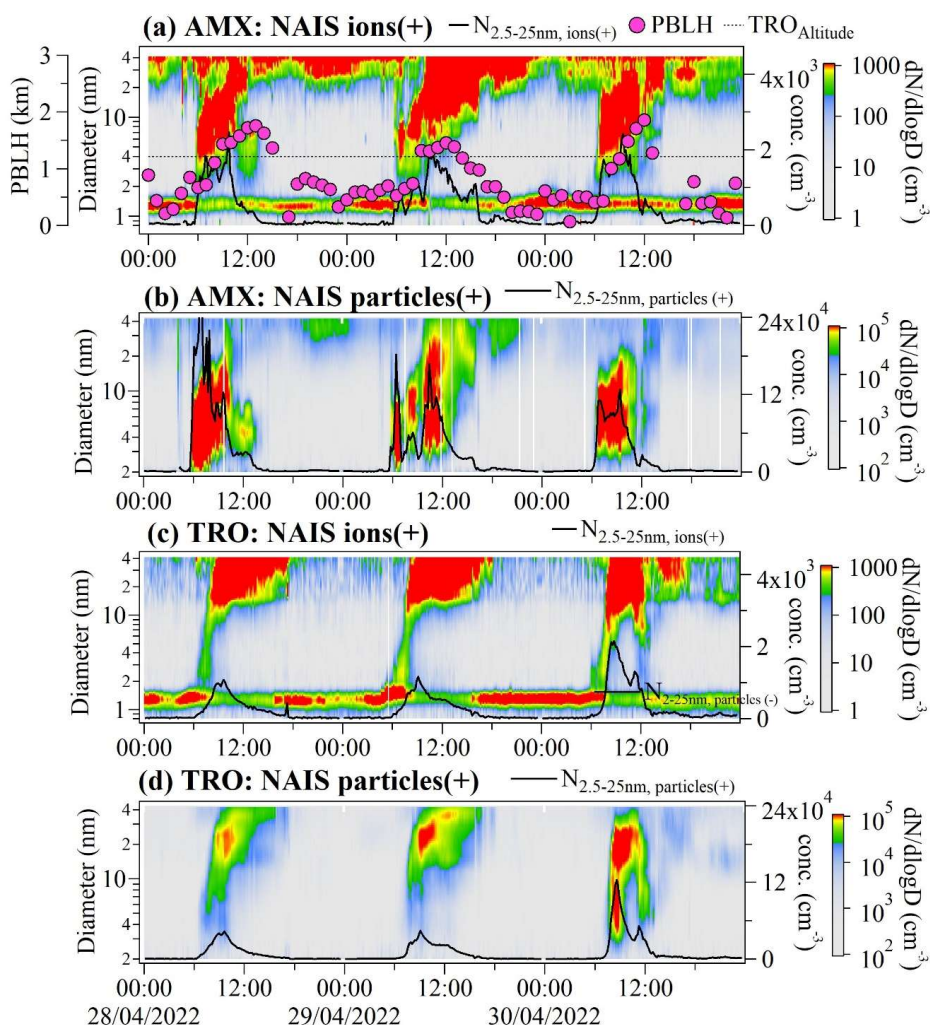
273 Three-day backward airmass trajectories arriving at 1000 m a.m.s.l. and 2000 m a.m.s.l. to  
274 AMX and TRO, respectively, during 6 - 12 UTC were determined using the National Oceanic  
275 and Atmospheric Administration (NOAA) ARL PC-version HYbrid SingleParticle Lagrangian  
276 Integrated Trajectory (HYSPLIT) transport and dispersion model (Draxler and Rolph, 2010),  
277 using 0.25 degree gridded wind fields from the Global Forecast System (GFS).

278

279 **3 Results and Discussion**

280 **3.1 NPF event frequency and characteristics**

281 The temporal evolution of positive ion and particle number size distributions at both sites  
282 (AMX and TRO) for the year 2022 are shown in Fig S1. Ion and particle number concentrations  
283 are generally higher at AMX than at TRO. Figure 2 shows the concurrent evolution of ion and  
284 particle number size distributions and number concentrations for observed typical NPF events  
285 at both sites and PBLH at the AMX site from 28 - 30 April 2022. The ion and particle number  
286 concentrations are two-fold higher at the AMX site as compared to the TRO site. While larger  
287 diameter background particles were continuously present at the AMX site, they were absent at  
288 the TRO site, suggesting that NPF events may be the major source of larger diameter particles  
289 in the Aitken mode at the TRO site (Fig. 2 and S1). Furthermore, the banana-shaped aerosol  
290 formation and growth pattern were significantly broader below 10 nm at the AMX site  
291 compared to the TRO site, suggesting that the intense NPF most likely lasted longer and the  
292 precursor vapour supply was sustained for a longer duration at AMX than at TRO. The PBLH  
293 was higher than the altitude of the TRO site, possibly indicating that the concurrent occurrence  
294 of NPF events at TRO was influenced by the evolution of the PBL (see section 3.3).



295

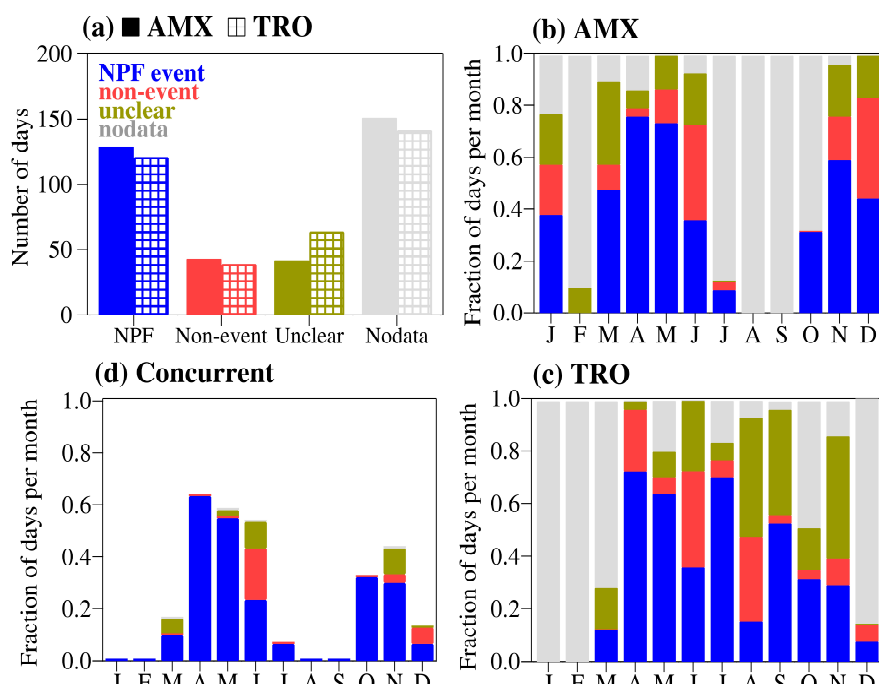
296 **Figure 2.** Time evolution of 10-minute averaged number size distributions of positive polarity  
 297 ions and total particles at AMX (a, b) and TRO (c, d), respectively, measured with NAIS from  
 298 28 April to 30 April 2022. The ion and particle number concentrations in the mobility diameter  
 299 range from 2.5 to 25 nm are shown by a solid black line. The PBLH at AMX above the ground  
 300 and the altitude of the TRO site above AMX are indicated by magenta colour dots and a black  
 301 colour dotted line, respectively.

302

303 Figure 3a shows the occurrence frequency of different types of event days at both AMX and  
 304 TRO sites. At AMX, NPF events were observed on 129 days (35.34%), 43 days did not have  
 305 signs of NPF (Non-events, 11.78%), while 42 days (11.51%) were unclear and there were no



306 valid measurements on 151 days (41.37%) during the calendar year of 2022. At TRO, NPF  
 307 events were observed on 121 days (33.16%), 39 days did not show NPF (non-events, 10.68%),  
 308 64 days were unclear (17.53%), and there were no valid measurements on 141 days (38.63%).  
 309 Out of the total observed NPF events at AMX (129 days out of 214 valid observation days,  
 310 60%) and at TRO (121 days out of 224 valid observation days, 54%), NPF events  
 311 were observed concurrently on 69 days at both sites (Table S1), indicating that the remaining  
 312 NPF events occur in different air masses at these sites even with the close proximity of sites  
 313 (approximately 20 km). The NPF frequency at the AMX site was the highest during spring as  
 314 compared to the rest of the year, analogous to the previous study at AMX (Baalbaki et al.,  
 315 2021) and other closest Eastern Mediterranean site, Finokalia atmospheric observation station,  
 316 in Crete (Kalivitis et al., 2019). The NPF frequency at the TRO site appears to be the highest  
 317 during spring, although the NPF frequency in July was comparable. The gaps in observational  
 318 data limit a detailed discussion of the seasonal characteristics of NPF events at both sites,  
 319 however, the concurrent observations, covering over 60% at both sites, are sufficient to assess  
 320 the impact of PBL evolution on NPF events at the TRO site.  
 321



322 **Figure 3.** (a) Number of days of different event types at both AMX and TRO sites, (b)  
 323 occurrence frequency (in fraction of days per month calculated as the number of event days  
 324



325 divided by the total number of calendar days in the month) of different event types at AMX,  
326 (c) same as (b) but for TRO, and (d) same as (b) but for concurrent days of NPF events, non-  
327 events and unclear days at both AMX and TRO sites, excludes individual different events types  
328 and nodata.

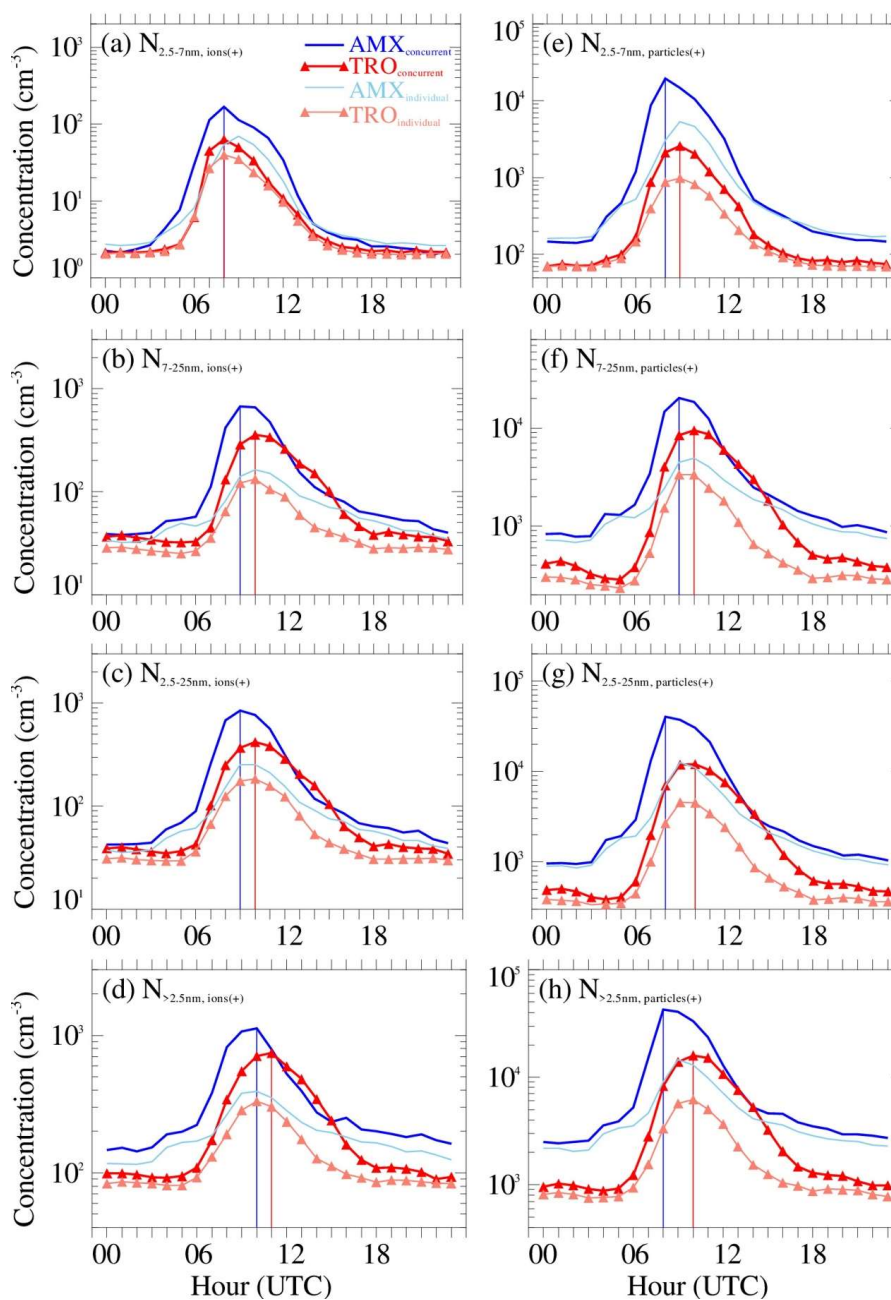
329

### 330 **3.2 Diurnal variation in positive polarity size-segregated ion and total particle number** 331 **concentrations, NPF events start-time and mode diameter**

332 Figure 4 shows the diurnal variation of size-segregated ion and particle number concentrations  
333 for positive polarity (see Fig. S2 for negative polarity) for concurrent NPF events observed at  
334 both sites as well as NPF events observed individually at each site. We used four size classes:  
335 2.5-7 nm, 7-25 nm, 2.5-25 nm, and >2.5 nm for both ions and particles. Ion and particle number  
336 concentrations exhibit similar diurnal cycles, with the highest concentrations occurring  
337 between 06:00 and 14:00 UTC, as NPF is predominately a daytime phenomenon driven by  
338 photochemistry in the presence of solar radiation (Asmi et al., 2011; Jokinen et al., 2017;  
339 Kanawade et al., 2012; Kerminen et al., 2018; Z. Wu et al., 2007). The noontime peak in size-  
340 segregated ion and particle number concentrations indicates the importance of photochemistry  
341 for NPF events at AMX and TRO sites. The concurrent peaks in temperature and solar radiation  
342 are also visible (Fig. S3a, b) and in the key aerosol precursors required for the initiation of  
343 aerosol formation, such as sulfur dioxide as compared to non-events (Fig. S3c). The low  
344 relative humidity (Fig. S3d), higher ozone concentrations (Fig. S3e), and sustained wind speed  
345 (Fig. S3f) as compared to non-events further indicate environmentally favourable conditions  
346 to promote particle formation and growth. Continuous observations of columnar aerosols from  
347 sunphotometers in AMX and TRO (AERONET) show that aerosol loading is higher at AMX  
348 compared to TRO throughout the year (Fig. S4a). Additionally, the higher value of the  
349 Ångström exponent at TRO than at AMX possibly suggests that NPF processes are the  
350 dominant source of these aerosol particles at TRO (Fig. S4b), especially in winter when the  
351 site is mostly in the free troposphere (see section 3.3). Furthermore, the absence of traffic-  
352 induced morning and evening peaks in size-segregated ion and particle number concentrations  
353 suggests that both sites are not influenced by local traffic emissions (Fig. 4). The blue and red  
354 vertical lines in Figure 4 indicate the occurrence times of peak concentrations for concurrent  
355 NPF events at AMX and TRO, respectively. The peak was consistently shifted to the right at  
356 the TRO site, except for intermediate ions (2.5–7 nm). This shift suggests a temporal delay of  
357 NPF events compared to AMX. This variation could reflect differences in local atmospheric  
358 dynamics, such as PBL evolution alongside aerosol precursors required for aerosol formation



359 and growth. When mountain sites experience daytime evolution of the PBL, a similar diurnal  
360 cycle of aerosol properties, to that of lower-altitude sites, is typically observed (Collaud Coen  
361 et al., 2018). Therefore, we hypothesise that the NPF event is detected earlier at the AMX site,  
362 shortly after sunrise, coinciding with an increase in temperature that drives the evolution of the  
363 PBL up to the height of the TRO site. The evolution of the PBL may carry precursor gases and  
364 aerosols up to the TRO site altitude, resulting in a later starting time of NPF events there.  
365



366

367 **Figure 4.** Median diurnal variation of positive polarity ion (a-d) and particle (e-h) size-  
368 segregated (2.5 - 7 nm, 7 - 25 nm, 2.5 - 25 nm, and >2.5 nm) number concentrations observed  
369 on concurrent NPF events at AMX (dark blue thick line) and TRO (dark red thick line). The  
370 light blue and light red thin lines are for NPF events observed individually at AMX and TRO,



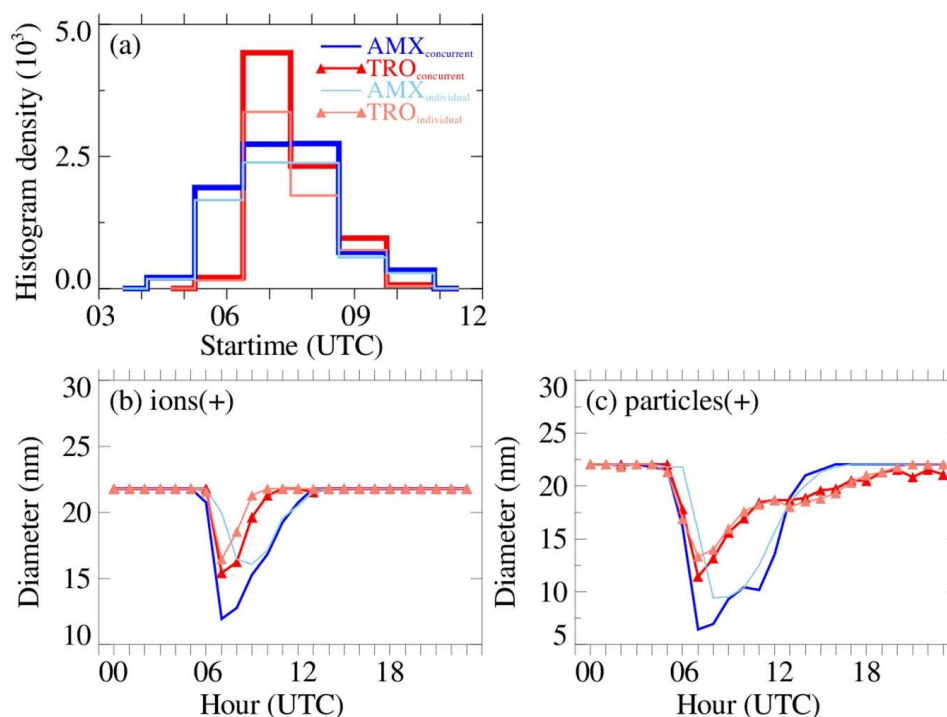
371 respectively. The blue and red vertical lines indicate the times at which the peak concentrations  
372 for concurrent NPF events were observed at AMX and TRO, respectively.

373

374 The peak in size-segregated ion and particle number concentrations exhibited a time lag of 1-  
375 2 hours for concurrent NPF events at both sites. In contrast, the peak concentrations occurred  
376 at the same time of day for individual NPF events at each site, implying a uniform influence of  
377 local-to-regional atmospheric conditions on the particle formation process. Further, ion and  
378 particle number concentrations were higher during concurrent NPF events observed at both  
379 AMX and TRO, compared to those observed at TRO alone. To further substantiate our  
380 hypothesis, we obtained start-time of NPF events, as well as the ion and particle mode diameter.  
381 The start-times indicate the approximate initiation time of NPF events, while the mode  
382 diameter provides insight into the evolution of particle size distributions in the atmosphere,  
383 (Figs. 5 and S5). The histogram of NPF start-times indicates that NPF events at the TRO site  
384 were consistently detected with a time lag of ~1 hour compared to AMX (Fig. 5a). At 7:00  
385 UTC, the particle (ion) mode diameters at AMX and TRO were about 6.5 nm (11.9 nm) and  
386 11.5 nm (15.5 nm), respectively (Fig. 5b, 5c). Considering the time lag of 1 hour between these  
387 sites, the particle growth rate can be estimated as ~5 nm/h, which is comparable to the  
388 calculated mean growth rate of particles (~7 nm/h) at the AMX site (Baalbaki et al., 2021). The  
389 lower particle mode diameter at AMX, coupled with a broader dip, in contrast to the higher  
390 mode diameter and narrower dip at TRO, suggests more sustained aerosol formation at AMX  
391 than at TRO. This corroborates with the results presented in Figure 2 showing that sub-10 nm  
392 particles were present for a longer time at AMX than at the TRO. This can result in the transport  
393 of growing sub-10nm particles from the lower-altitude AMX site to the higher-altitude TRO  
394 site by up-valley winds or vertical mixing. Therefore, we next examine PBL evolution and its  
395 influence on the TRO mountain site.

396





397

398 **Figure 5.** Median diurnal variation of positive polarity (a) ion and (b) particle mode diameter  
399 for the observed concurrent NPF events at AMX (dark blue) and TRO (dark red). (c) Histogram  
400 density of NPF events start-time. The light blue and light red coloured thin lines are for NPF  
401 events observed individually at AMX and TRO, respectively.

402

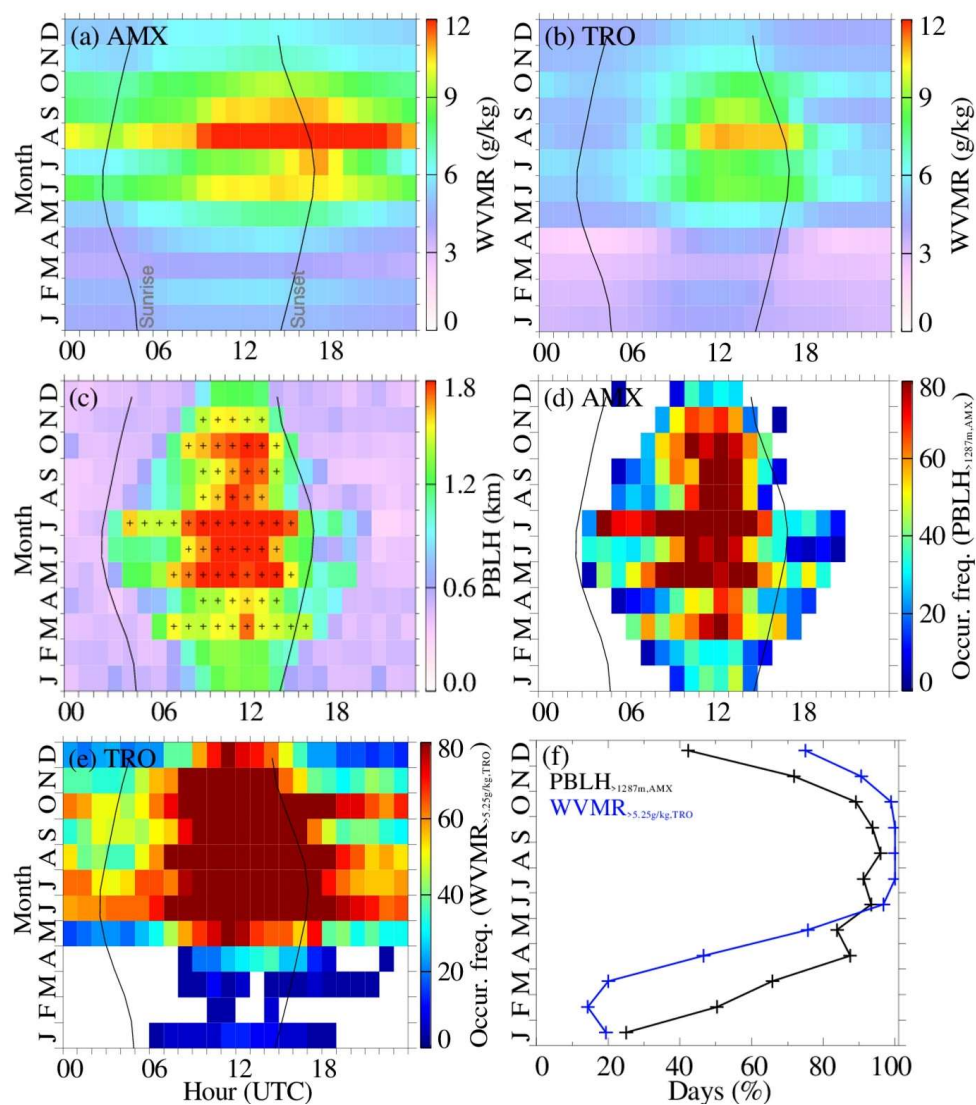
### 403 3.3 Examining PBL evolution and its influence on the TRO site

404 The vertical evolution of the PBL significantly influences meteorological and environmental  
405 factors, such as near-surface pollutant concentrations, wind velocity, and turbulent exchange  
406 of momentum, heat, and moisture (Stull, 1988). The most accurate and common measurements  
407 of thermodynamic profiles are achieved using radiosondes, but the temporal resolution is too  
408 sparse to detect the evolution of the diurnal structure of PBL. Ground-based remote sensing  
409 techniques fill this gap, providing high temporal resolution information, such as sound  
410 detection and ranging (SODAR), radio acoustic sounding system (RASS), and light detecting  
411 and ranging (LiDAR) (Kotthaus et al., 2023). Here, we used ceilometer measurements from a  
412 lower-altitude site (AMX) along with WVMR, passive tracers of PBL dynamics, from both  
413 sites to examine the diurnal evolution of the PBL and assess its impact on the mountain site  
414 (TRO). Figure 6 shows the monthly median diurnal variation of WVMR at both sites, PBLH



415 at AMX, and the estimates for the influence of the PBL evolution on the TRO site. The monthly  
416 median diurnal variation of WVMR illustrates the probable mixing of air between the lower-  
417 altitude AMX site and the mountain TRO site (e.g. up-valley wind or vertical mixing) except  
418 during late winter and early spring (Fig. 6a, b). Concurrently, the WVMRs at the TRO site  
419 were consistently lower than the threshold of 5.25 g/kg during late winter and early spring,  
420 suggesting that the site is primarily influenced by free tropospheric (FT) air (Fig. 6b). The  
421 pattern was reinforced by the analysis of PBLH, exhibiting similar seasonal cycle. The  
422 monthly median PBLH was found to be lower than the altitude of the TRO site during late  
423 winter and early spring, and higher for the remainder of the year. We further calculated the  
424 occurrence frequency of PBLH at AMX exceeding the altitude of the TRO site (1287 m above  
425 AMX) and WVMR at TRO exceeding a threshold value of 5.25 g/kg. The occurrence  
426 frequencies demonstrate the observed seasonal and diurnal patterns in PBL influence on the  
427 TRO site (Figs. 6d, 6e). This suggests that the TRO site is periodically influenced by the PBL  
428 evolution during later winter and early spring, whereas it is primarily within the PBL for the  
429 remainder of the year. Lastly, Figure 6f shows the monthly fraction of days when the TRO site  
430 is influenced by the evolution of PBL. The TRO site is within the PBL on approximately 25%  
431 of days during late winter and early spring, increasing to >80% for the remainder of the year.  
432 The concurrent patterns observed in these tracers (PBLH and WVMR) suggest that the TRO  
433 site is impacted by the transport of polluted air from lower-elevation regions, possibly through  
434 vertical mixing or up-valley wind. Previous studies have demonstrated that up-valley winds  
435 can facilitate the upward movement of aerosol precursors, which can rapidly form a large  
436 number of new aerosol particles, and pre-existing particles from lower-altitude regions to  
437 mountain measurement sites, particularly within an elevated PBL (Bianchi et al., 2021; Hooda  
438 et al., 2018; Sebastian et al., 2021; Cusack et al., 2013).

439



440

441 **Figure 6.** Monthly median diurnal variation of WVMR at (a) AMX, (b) TRO, and (c) PBLH  
442 at AMX. The pixels with a plus sign in (c) indicate the times of the day when PBLH is higher  
443 than the altitude of the TRO site (1287 m above the AMX site). (d) monthly median diurnal  
444 variation of the occurrence frequency of PBLH higher than the altitude of the TRO site, (e)  
445 monthly median diurnal variation of the occurrence frequency of WVMR > 5.25 g/kg at TRO,  
446 indicative of the PBL evolution up to the altitude of the TRO site, and (f) monthly fraction of  
447 days the TRO site is influenced by the evolution of PBL as illustrated by PBLH higher than

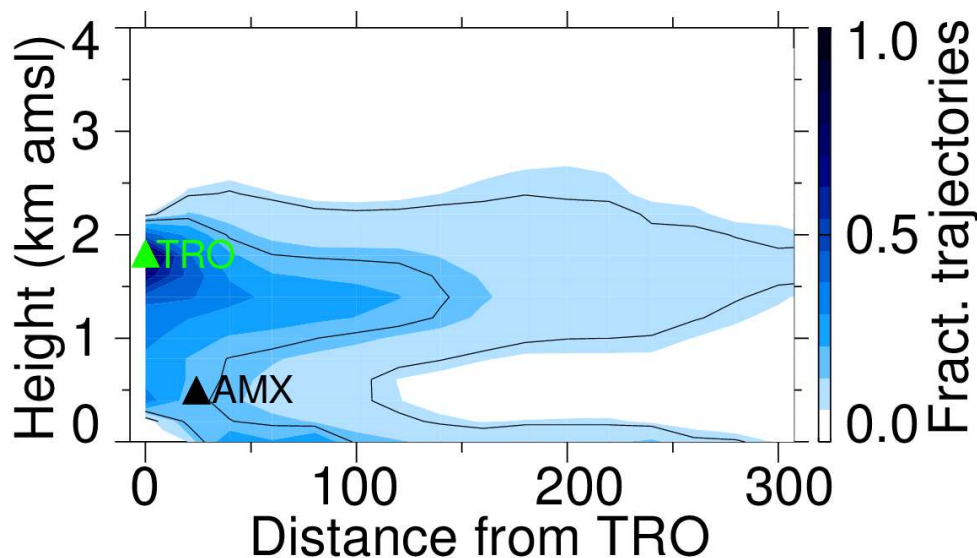


448 the altitude of the TRO site and  $WVMR > 5.25$  g/kg at TRO. The grey-coloured thin lines in  
449 (a)-(e) indicate UTC sunrise and sunset times.

450

451 To further substantiate our hypothesis, we examined the air mass history at the TRO site during  
452 observed concurrent NPF event days. Figure 7 shows the vertical cross-section of the fraction  
453 of air mass backward trajectories arriving at the TRO for observed concurrent NPF events. A  
454 large fraction of air masses had spent considerable time within the PBL before ascending to  
455 the altitude of the TRO site during concurrent NPF events at TRO. The monthly averaged  
456 airmass backward trajectories on concurrent NPF events showed that the free tropospheric air  
457 masses descended into the PBL upon entering the Mediterranean Sea, then they travelled along  
458 the surface towards the AMX site (Fig. S6) and eventually ascended to the TRO site altitude  
459 and above in response to the evolving PBL during the day (Fig. 7). The amplitude of the diurnal  
460 pattern of aerosol properties is the highest for the concurrent NPF events (Figs. 4, 5), further  
461 substantiating that the TRO site experiences daytime evolution of the PBL, analogous to a  
462 previous study demonstrating the daytime PBL influence due to vertical mixing (Collaud Coen  
463 et al., 2018). On the other hand, the airmass backward trajectories on individual NPF event  
464 days at these sites show distinct air mass history (Fig. S7)

465



466

467 **Figure 7.** Vertical cross-section of the fraction of airmass backward trajectories arriving at the  
468 TRO site (6 - 12 UTC) for the observed concurrent NPF events. The green and black upward  
469 triangle indicates TRO and AMX elevation above mean sea level, respectively.



470 **4. Discussions**

471 The frequency of occurrence of NPF events was comparable between AMX (a lower-altitude  
472 rural site) and TRO (a higher-altitude mountain site) in Cyprus, as opposed to the findings of  
473 Boulon et al. (2011) in Central France, where NPF events were more frequent at a mountain  
474 site (the Puy de Dôme station, 1465 m a.m.s.l.) than at a nearby rural lower-altitude site (the  
475 Opme station, 660 m a.m.s.l., about 12 km southeast of the Puy de Dôme station). The exact  
476 reasons for the higher frequency of NPF events at Puy de Dôme remain unclear. However,  
477 Farah et al. (2018) used PBL tracers, such as particle size distribution and black carbon  
478 concentrations, to distinguish between free-tropospheric and PBL air masses at Puy de Dôme.  
479 They found that the Puy de Dôme station is within the PBL 50% of the time during the winter  
480 and up to 97% during the summer. Since most mountain sites are typically within the PBL  
481 during the day, when NPF occurs, it is important to investigate whether the mountain site is  
482 influenced by the evolving PBL. The AMX and TRO sites are also located close to each other,  
483 approximately 20 km apart, yet we observed similar NPF frequencies at both (Fig. 3a), unlike  
484 in Central France (Boulon et al., 2011). About half of the NPF events occurred simultaneously  
485 at both sites (Fig. 3d), particularly when the airmasses originated from the northwest to  
486 northeast corridor relative to the TRO site. At measurement sites situated above 1000 m a.s.l.,  
487 higher condensation sink tend to favour NPF, likely due to the presence of precursor gases  
488 needed to initiate nucleation and early growth (Sellegrì et al., 2019), which is thought to be  
489 linked to vertically elevated precursor gases that promote particle formations and growth (in  
490 this case, Fig. S3c shows higher SO<sub>2</sub> concentrations during NPF events than non-events at  
491 TRO). Measurements from a remote background site in the western Himalayas also indicated  
492 that NPF was favoured under the influence of anthropogenic plumes with a higher condensation  
493 sink indicative of the precursor- and aerosol-laden air (Sebastian et al., 2021). Measurements  
494 from a mountain site (Mount Heng, Huan Province) in South China further demonstrated that  
495 NPF events in the remote ambient atmosphere are favoured during heavy dust episodes mixed  
496 with anthropogenic pollution (Nie et al., 2014). This suggests that the balance between  
497 precursor vapours and pre-existing particles in polluted air masses determines when NPF is  
498 favoured in the atmosphere (Kanawade et al., 2021; Hyvärinen et al., 2010).

499

500 A previous study demonstrated that the 30-minute time lag between black carbon  
501 concentrations and the cluster ion mode suggests that nucleation processes may be initiated at  
502 the interface between the PBL and the free troposphere (Sellegrì et al., 2019). However, the 1–  
503 2 hour time lag and the higher magnitude of aerosol properties at the AMX site compared to



504 TRO (Figs. 4, S2, S3c, and S4a) suggest nucleation processes likely occurred within the well-  
505 mixed PBL. Crumeyrolle et al. (2010) also showed that nucleation occurs within the boundary  
506 layer, with the vertical extension of NPF events not exceeding the boundary layer's top. This  
507 can be explained by turbulent mixing leading to local supersaturation of condensable vapours  
508 and the dispersion of pre-existing particles, which in turn could enhance the nucleation process  
509 within the PBL. Even at higher-altitude sites like the Jungfraujoch station (3580 m a.m.s.l.),  
510 studies have shown that NPF events can occur within free tropospheric air masses, provided  
511 these air masses were in contact with the PBL during a certain time frame (Bianchi et al., 2016;  
512 Tröstl et al., 2016b). Carnerero et al. (2018) also showed that ultrafine particles are formed  
513 within the mixed layer, and as this layer expands, these particles are subsequently detected at  
514 higher altitudes within the PBL. On the contrary, Platis et al. (2016) provided observational  
515 evidence of the inversion layer facilitating thermodynamic conditions for NPF at elevated  
516 altitudes within the PBL, and subsequently, these particles moved toward the ground. Several  
517 studies also showed that NPF events preferentially take place in the upper free troposphere  
518 (Clarke and Kapustin, 2002; Hamburger et al., 2011; Rose et al., 2015), or at the interface  
519 between the PBL and the free troposphere (Wehner et al., 2015). We also found NPF events at  
520 TRO alone may be taking place in the free troposphere or at the interface between the PBL and  
521 the free troposphere (Fig. S7), which is yet to be investigated. Nonetheless, several researchers  
522 reported NPF events in the free troposphere, such as pure-biogenic NPF driven by natural  
523 biogenic emission in the upper troposphere (above 13 km) (Zhao et al., 2020), in cloud outflows  
524 (Kanawade and Tripathi, 2006; Clarke et al., 1998), and in the upper troposphere and lower  
525 stratosphere (Lee et al., 2008; Brock et al., 1995; Schröder and Ström, 1997). This underscores  
526 the complexity of NPF processes, which are also influenced by altitude in addition to  
527 atmospheric conditions, suggesting that the vertical extent of nucleation processes is poorly  
528 studied.

529

## 530 **5. Conclusions**

531 This work presents the concurrent observations of ion and particle size distributions from a  
532 rural background lower-altitude site (Agia Marina Xyliatou, 532 m a.m.s.l.) and a higher-  
533 altitude background mountain site (Troodos, 1819 m a.m.s.l.) in Cyprus for the year 2022. We  
534 investigated the influence of boundary layer evolution on the NPF occurrence at a background  
535 mountain site, TRO. We found that the NPF event frequency was comparable between AMX  
536 (129 days out of 214 valid observation days, 60%) and TRO (121 days out of 224 valid  
537 observation days, 54%). Out of these, NPF events occurred concurrently at both sites on 69



538 days. Typical NPF events at AMX and TRO exhibited distinct patterns, with AMX showing a  
539 significantly longer-lasting banana-shaped distribution below 10 nm diameter compared to  
540 TRO, suggesting differences in the supply of precursor vapours. During concurrent NPF  
541 events, the smaller mode diameter at the AMX site implies that nucleation processes occur  
542 nearby, while the particles have grown larger before they are detected at TRO.

543

544 By combining measurements from the higher-altitude TRO site with those from the lower-  
545 altitude AMX site, we were able to investigate the influence of evolving PBL on the nucleation  
546 processes in this remote mountainous region. For this, we used ceilometer measurements from  
547 AMX along with WVMR, passive tracers of PBL dynamics, from both sites to examine the  
548 diurnal evolution of the PBL. Our analyses indicated that the TRO site is within the PBL on  
549 approximately 25% of days during late winter and early spring, increasing to >80% of days for  
550 the remainder of the year. We used 69 days of concurrent NPF events days and compared them  
551 with individual NPF events at both sites. The peak in size-segregated ion and particle number  
552 concentrations occurred at the same time of day for individual NPF events at each site, implying  
553 a uniform influence of local-to-regional atmospheric conditions on the particle formation  
554 processes. For concurrent NPF events, the peak was observed at the lower-altitude site first,  
555 followed by a 1-2 hour time delay at the mountain site, TRO, suggesting the vertical extent of  
556 the nucleation process within the PBL. In these cases, NPF events at TRO are linked to the  
557 evolving PBL since the nucleation is detected at TRO when the PBL extends over the altitude  
558 of the TRO site. This was substantiated by a 1-hour delay in the NPF events start-time and a  
559 relatively larger particle mode diameter at TRO. This suggests that the transport of precursor  
560 vapour-laden air from lower-altitude regions, likely driven by vertical mixing or up-valley  
561 winds, might play a significant role in the aerosol formation process in the higher-altitude site.  
562 The airmass history for concurrent NPF events revealed that a significant fraction of the  
563 airmass trajectories had previously been in contact with the PBL before reaching the TRO site.  
564 This suggests the vertical extent of NPF processes within the evolving PBL, though this  
565 requires further critical investigation. The influence of evolving PBL at a mountain site in this  
566 study reflects similarities with those reported in earlier studies, showing observed NPF events  
567 at a higher-altitude site, whether within or above PBL, have always been linked with the PBL  
568 (Bianchi et al., 2016; Carnerero et al., 2018; Sebastian et al., 2021; Sellegri et al., 2019; Bianchi  
569 et al., 2021; Hooda et al., 2018), except those observed in the middle-upper troposphere and  
570 stratosphere or convective cloud outflows.



571 An improved understanding of the exchange of energy, moisture, and atmospheric constituents,  
572 including aerosols, between the PBL and the atmosphere above is crucial for climate models.  
573 However, the complex nature of the PBL dynamics hampers the current understanding of  
574 atmospheric processes such as aerosol-induced changes in radiative balance, cloud cover,  
575 precipitation, and even regional circulation patterns, which have feedback with regional and  
576 climate processes. Therefore, the process-level understanding of atmospheric processes and  
577 their feedback such as airborne production of aerosols, within the boundary layer is crucial for  
578 future climate prediction.

579

#### 580 ***Data availability***

581 In-situ measurements of ion and particle size distributions, meteorological parameters and  
582 gases, and screened planetary boundary layer data can be accessed at Zenodo (add citations  
583 here). The ceilometer data can also be viewed at <https://e-profile.eu/> (last accessed 22 October  
584 2024). ERA-5 boundary layer height data is publicly available from  
585 <https://cds.climate.copernicus.eu/datasets/reanalysis-era5-single-levels> (last accessed 22  
586 October 2024). AERONET aerosol optical depth and Ångström exponent data are available  
587 publicly to download from <https://aeronet.gsfc.nasa.gov/> (last accessed 22 October 2024)

588

#### 589 ***Author contributions***

590 FM, JS, MK, KL and TJ designed the experiments and ND, AP, RB, MP carried them out. ND,  
591 VPK and AP analysed the data. ND, VPK and TJ prepared the manuscript with contributions  
592 from all co-authors.

593

#### 594 ***Competing interests.***

595 At least one of the (co-)authors is a member of the editorial board of Aerosol Research. The  
596 authors declare that they have no conflict of interest.

597

#### 598 ***Acknowledgements.***

599 This work has been supported by the European Union's Horizon 2020 Research and Innovation  
600 Programme under grant agreement No. 856612 and the Cyprus Government. TJ acknowledges  
601 the funding support by the European Union ERC-2022-STGERC-BAE-Project: 101076311.  
602 Views and opinions expressed are however those of the author(s) only and do not necessarily  
603 reflect those of the European Union or the European Research Council Executive Agency.  
604 Neither the European Union nor the granting authority can be held responsible for them. The





605 authors thank the University of Helsinki, INAR/Physics for support and instrumentation. The  
606 authors also thank the technical support team; Nikoleta Lekaki, Moreno Parolin, and Rafail  
607 Konatzii for the technical support in maintaining field stations. The authors thank all the past  
608 and present personnel who contributed to the field measurements within the EMME project.

609

## 610 References

611 Aktypis, A., Kaltsonoudis, C., Skyllakou, K., Matrali, A., Vasilakopoulou, C. N., Florou, K.,  
612 and Pandis, S. N.: Infrequent new particle formation in a coastal Mediterranean city during the  
613 summer, *Atmos. Environ.*, 302, 119732, <https://doi.org/10.1016/j.atmosenv.2023.119732>,  
614 2023.

615 Aktypis, A., Kaltsonoudis, C., Patoulias, D., Kalkavouras, P., Matrali, A., Vasilakopoulou, C.  
616 N., Kostenidou, E., Florou, K., Kalivitis, N., Bougiatioti, A., Eleftheriadis, K., Vratolis, S.,  
617 Gini, M. I., Kouras, A., Samara, C., Lazaridis, M., Chatoutsidou, S. E., Mihalopoulos, N., and  
618 Pandis, S. N.: Significant spatial gradients in new particle formation frequency in Greece  
619 during summer, *Atmos. Chem. Phys.*, 24, 65-84, <https://doi.org/10.5194/acp-24-65-2024>,  
620 2024.

621 Asmi, E., Kivekäs, N., Kerminen, V.-M., Komppula, M., Hyvärinen, A.-P., Hatakka, J.,  
622 Viisanen, Y., & Lihavainen, H.: Secondary new particle formation in Northern Finland Pallas  
623 site between the years 2000 and 2010. *Atmos. Chem. Phys.*, 11(24), 12959–12972.  
624 <https://doi.org/10.5194/acp-11-12959-2011>, 2011

625 Baalbaki, R., Pikridas, M., Jokinen, T., Laurila, T., Dada, L., Bezantakos, S., Ahonen, L.,  
626 Neitola, K., Maisser, A., Bimenyimana, E., Christodoulou, A., Unga, F., Savvides, C.,  
627 Lehtipalo, K., Kangasluoma, J., Biskos, G., Petäjä, T., Kerminen, V. M., Sciare, J., and  
628 Kulmala, M.: Towards understanding the characteristics of new particle formation in the  
629 Eastern Mediterranean, *Atmos. Chem. Phys.*, 21, 9223-9251, <https://doi.org/10.5194/acp-21-9223-2021>, 2021.

631 Bianchi, F., Junninen, H., Bigi, A., Sinclair, V. A., Dada, L., Hoyle, C. R., Zha, Q., Yao, L.,  
632 Ahonen, L. R., Bonasoni, P., Buenrostro Mazon, S., Hutterli, M., Laj, P., Lehtipalo, K.,  
633 Kangasluoma, J., Kerminen, V. M., Kontkanen, J., Marinoni, A., Mirme, S., Molteni, U.,  
634 Petäjä, T., Riva, M., Rose, C., Sellegri, K., Yan, C., Worsnop, D. R., Kulmala, M.,  
635 Baltensperger, U., and Dommen, J.: Biogenic particles formed in the Himalaya as an important  
636 source of free tropospheric aerosols, *Nat. Geosci.*, 14, 4-9, <https://doi.org/10.1038/s41561-020-00661-5>, 2021.

638 Bianchi, F., Tröstl, J., Junninen, H., Frege, C., Henne, S., Hoyle, C. R., Molteni, U., Herrmann,  
639 E., Adamov, A., Bukowiecki, N., Chen, X., Duplissy, J., Gysel, M., Hutterli, M., Kangasluoma,  
640 J., Kontkanen, J., Kürten, A., Manninen, H. E., Münch, S., Peräkylä, O., Petäjä, T., Rondo, L.,  
641 Williamson, C., Weingartner, E., Curtius, J., Worsnop, D. R., Kulmala, M., Dommen, J., and  
642 Baltensperger, U.: New particle formation in the free troposphere: A question of chemistry and  
643 timing, *Science*, 352, 1109-1112, <https://doi.org/10.1126/science.aad5456>, 2016.

644 Bimenyimana, E., Pikridas, M., Oikonomou, K., Iakovides, M., Christodoulou, A., Sciare, J.,  
645 and Mihalopoulos, N.: Fine aerosol sources at an urban background site in the Eastern



- 646 Mediterranean (Nicosia; Cyprus): Insights from offline versus online source apportionment  
647 comparison for carbonaceous aerosols, *Sci. Total Environ.*, 893, 164741,  
648 <https://doi.org/10.1016/j.scitotenv.2023.164741>, 2023.
- 649 Boulon, J., Sellegri, K., Hervo, M., Picard, D., Pichon, J. M., Fréville, P., and Laj, P.:  
650 Investigation of nucleation events vertical extent: a long term study at two different altitude  
651 sites, *Atmos. Chem. Phys.*, 11, 5625-5639, <https://doi.org/10.5194/acp-11-5625-2011>, 2011.
- 652 Brilke, S., Fölker, N., Müller, T., Kandler, K., Gong, X., Peischl, J., Weinzierl, B., and Winkler,  
653 P. M.: New particle formation and sub-10 nm size distribution measurements during the A-  
654 LIFE field experiment in Paphos, Cyprus, *Atmos. Chem. Phys.*, 20, 5645-5656,  
655 <https://doi.org/10.5194/acp-20-5645-2020>, 2020.
- 656 Brock, C. A., Hamill, P., Wilson, J. C., Jonsson, H. H., and Chan, K. R.: Particle Formation in  
657 the Upper Tropical Troposphere: A Source of Nuclei for the Stratospheric Aerosol, *Science*,  
658 270, 1650-1653, <https://doi.org/10.1126/science.270.5242.1650>, 1995.
- 659 Buck, A. L.: New Equations for Computing Vapor Pressure and Enhancement Factor, *J. Appl.*  
660 *Meteorol. Climatol.*, 20, 1527-1532, [https://doi.org/10.1175/1520-0450\(1981\)020<1527:NEFCVP>2.0.CO;2](https://doi.org/10.1175/1520-0450(1981)020<1527:NEFCVP>2.0.CO;2), 1981.
- 662 Buenrostro Mazon, S., Riipinen, I., Schultz, D. M., Valtanen, M., Dal Maso, M., Sogacheva,  
663 L., Junninen, H., Nieminen, T., Kerminen, V.-M., and Kulmala, M.: Classifying previously  
664 undefined days from eleven years of aerosol-particle-size distribution data from the SMEAR  
665 II station, Hyytiälä, Finland, *Atmos. Chem. Phys.*, 9, 667-676, <https://doi.org/10.5194/acp-9-667-2009>, 2009.
- 667 Carnerero, C., Pérez, N., Reche, C., Ealo, M., Titos, G., Lee, H. K., Eun, H. R., Park, Y. H.,  
668 Dada, L., Paasonen, P., Kerminen, V. M., Mantilla, E., Escudero, M., Gómez-Moreno, F. J.,  
669 Alonso-Blanco, E., Coz, E., Saiz-Lopez, A., Temime-Roussel, B., Marchand, N., Beddows, D.  
670 C. S., Harrison, R. M., Petäjä, T., Kulmala, M., Ahn, K. H., Alastuey, A., and Querol, X.:  
671 Vertical and horizontal distribution of regional new particle formation events in Madrid,  
672 *Atmos. Chem. Phys.*, 18, 16601-16618, <https://doi.org/10.5194/acp-18-16601-2018>, 2018.
- 673 Clarke, A. D. and Kapustin, V. N.: A Pacific Aerosol Survey. Part I: A Decade of Data on  
674 Particle Production, Transport, Evolution, and Mixing in the Troposphere *J. Atmos. Sci.*, 59,  
675 363-382, [https://doi.org/10.1175/1520-0469\(2002\)059<0363:APASPI>2.0.CO;2](https://doi.org/10.1175/1520-0469(2002)059<0363:APASPI>2.0.CO;2), 2002.
- 676 Clarke, A. D., Varner, J. L., Eisele, F., Mauldin, R. L., Tanner, D., and Litchy, M.: Particle  
677 production in the remote marine atmosphere: Cloud outflow and subsidence during ACE 1, *J.*  
678 *Geophys. Res.*103, 16397-16409, <https://doi.org/10.1029/97JD02987>, 1998.
- 679 Collaud Coen, M., Andrews, E., Aliaga, D., Andrade, M., Angelov, H., Bukowiecki, N., Ealo,  
680 M., Fialho, P., Flentje, H., Hallar, A. G., Hooda, R., Kalapov, I., Krejci, R., Lin, N. H.,  
681 Marinoni, A., Ming, J., Nguyen, N. A., Pandolfi, M., Pont, V., Ries, L., Rodríguez, S., Schauer,  
682 G., Sellegri, K., Sharma, S., Sun, J., Tunved, P., Velasquez, P., and Ruffieux, D.: Identification  
683 of topographic features influencing aerosol observations at high altitude stations, *Atmos.*  
684 *Chem. Phys.*, 18, 12289-12313, <https://doi.org/10.5194/acp-18-12289-2018>, 2018.
- 685 Crumeyrolle, S., Manninen, H. E., Sellegri, K., Roberts, G., Gomes, L., Kulmala, M., Weigel,  
686 R., Laj, P., and Schwarzenboeck, A.: New particle formation events measured on board the



- 687 ATR-42 aircraft during the EUCAARI campaign, *Atmos. Chem. Phys.*, 10, 6721-6735,  
688 <https://doi.org/10.5194/acp-10-6721-2010>, 2010.
- 689 Cusack, M., Alastuey, A., and Querol, X.: Case studies of new particle formation and  
690 evaporation processes in the western Mediterranean regional background, *Atmos. Environ.*, 81,  
691 651-659, <https://doi.org/10.1016/j.atmosenv.2013.09.025>, 2013.
- 692 Dal Maso, M., Kulmala, M., Riipinen, I., Wagner, R., Hussein, T., Aalto, P. P., and Lehtinen,  
693 K. E. J.: Formation and growth of fresh atmospheric aerosols: eight years of aerosol size  
694 distribution data from SMEAR II, Hyytiälä, Finland, *Boreal Env. Res.*, 10, 323-336, ISSN  
695 1239-6095, 2005.
- 696 Debevec, C., Sauvage, S., Gros, V., Sellegri, K., Sciare, J., Pikridas, M., Stavroulas, I.,  
697 Leonardis, T., Gaudion, V., Depelchin, L., Fronval, I., Sarda-Esteve, R., Baisnée, D., Bonsang,  
698 B., Savvides, C., Vrekoussis, M., and Locoge, N.: Driving parameters of biogenic volatile  
699 organic compounds and consequences on new particle formation observed at an eastern  
700 Mediterranean background site, *Atmos. Chem. Phys.*, 18, 14297-14325,  
701 <https://doi.org/10.5194/acp-18-14297-2018>, 2018.
- 702 Dinoi, A., Gulli, D., Weinhold, K., Ammoscato, I., Calidonna, C. R., Wiedensohler, A., and  
703 Contini, D.: Characterization of ultrafine particles and the occurrence of new particle formation  
704 events in an urban and coastal site of the Mediterranean area, *Atmos. Chem. Phys.*, 23, 2167-  
705 2181, <https://doi.org/10.5194/acp-23-2167-2023>, 2023.
- 706 Draxler, R. R. and Rolph, G. D.: HYSPLIT (HYbrid Single-Particle Lagrangian Integrated  
707 Trajectory) Model Access via NOAA ARL READY Website. NOAA Air Resources  
708 Laboratory, Silver Spring. <http://ready.arl.noaa.gov/HYSPLIT.php>, 2010.
- 709 Emeis, S., Jahn, C., Münkel, C., Münsterer, C., and Schäfer, K.: Multiple atmospheric layering  
710 and mixing-layer height in the Inn valley observed by remote sensing, *Meteorol. Z.*, 16, 415-  
711 424, <https://doi.org/10.1127/0941?2948/2007/0203>, 2007.
- 712 Farah, A., Freney, E., Chauvigné, A., Baray, J.-L., Rose, C., Picard, D., Colomb, A., Hadad,  
713 D., Abboud, M., Farah, W., and Sellegri, K.: Seasonal variation of aerosol size distribution data  
714 at the Puy de Dôme station with emphasis on the boundary layer/free troposphere segregation,  
715 *Atmosphere*, 9, 244, <https://doi.org/10.3390/atmos9070244>, 2018.
- 716 Gong, X., Wex, H., Müller, T., Wiedensohler, A., Höhler, K., Kandler, K., Ma, N., Dietel, B.,  
717 Schiebel, T., Möhler, O., and Stratmann, F.: Characterization of aerosol properties at Cyprus,  
718 focusing on cloud condensation nuclei and ice-nucleating particles, *Atmos. Chem. Phys.*, 19,  
719 10883-10900, [10.5194/acp-19-10883-2019](https://doi.org/10.5194/acp-19-10883-2019), 2019.
- 720 Gordon, H., Kirkby, J., Baltensperger, U., Bianchi, F., Breitenlechner, M., Curtius, J., Dias, A.,  
721 Dommen, J., Donahue, N. M., Dunne, E. M., Duplissy, J., Ehrhart, S., Flagan, R. C., Frege, C.,  
722 Fuchs, C., Hansel, A., Hoyle, C. R., Kulmala, M., Kürten, A., Lehtipalo, K., Makhmutov, V.,  
723 Molteni, U., Rissanen, M. P., Stozkhov, Y., Tröstl, J., Tsagkogeorgas, G., Wagner, R.,  
724 Williamson, C., Wimmer, D., Winkler, P. M., Yan, C., and Carslaw, K. S.: Causes and  
725 importance of new particle formation in the present-day and preindustrial atmospheres, *J.*  
726 *Geophys. Res.*, 122, 8739-8760, <https://doi.org/10.1002/2017jd026844>, 2017.



- 727 Gormley, P. G. and Kennedy, M.: Diffusion from a Stream Flowing Through a Cylindrical  
728 Tube, *Proc. R. Ir. Acad., Sect. A*, 52, 163-169, <https://www.jstor.org/stable/20488498>, 1949.
- 729 Hakala, S., Vakkari, V., Lihavainen, H., Hyvärinen, A. P., Neitola, K., Kontkanen, J.,  
730 Kerminen, V. M., Kulmala, M., Petäjä, T., Hussein, T., Khoder, M. I., Alghamdi, M. A., and  
731 Paasonen, P.: Explaining apparent particle shrinkage related to new particle formation events  
732 in western Saudi Arabia does not require evaporation, *Atmos. Chem. Phys.*, 23, 9287-9321,  
733 <https://doi.org/10.5194/acp-23-9287-2023>, 2023.
- 734 Hakala, S., Alghamdi, M. A., Paasonen, P., Vakkari, V., Khoder, M. I., Neitola, K., Dada, L.,  
735 Abdelmaksoud, A. S., Al-Jeelani, H., Shabbaj, I. I., Almeahadi, F. M., Sundström, A. M.,  
736 Lihavainen, H., Kerminen, V. M., Kontkanen, J., Kulmala, M., Hussein, T., and Hyvärinen, A.  
737 P.: New particle formation, growth and apparent shrinkage at a rural background site in western  
738 Saudi Arabia, *Atmos. Chem. Phys.*, 19, 10537-10555, [https://doi.org/10.5194/acp-19-10537-](https://doi.org/10.5194/acp-19-10537-2019)  
739 2019, 2019.
- 740 Hamburger, T., McMeeking, G., Minikin, A., Birmili, W., Dall'Osto, M., O'Dowd, C., Flentje,  
741 H., Henzing, B., Junninen, H., Kristensson, A., de Leeuw, G., Stohl, A., Burkhardt, J. F., Coe,  
742 H., Krejci, R., and Petzold, A.: Overview of the synoptic and pollution situation over Europe  
743 during the EUCAARI-LONGREX field campaign, *Atmos. Chem. Phys.*, 11, 1065-1082,  
744 <https://doi.org/10.5194/acp-11-1065-2011>, 2011.
- 745 Hersbach, H., Bell, B., Berrisford, P., Biavati, G., Horányi, A., Muñoz Sabater, J., Nicolas, J.,  
746 Peubey, C., Radu, R., Rozum, I., Schepers, D., Simmons, A., Soci, C., Dee, D., and Thépaut,  
747 J.-N.: ERA5 hourly data on pressure levels from 1940 to present. Copernicus Climate Change  
748 Service (C3S) Climate Data Store (CDS), <https://doi.org/10.24381/cds.bd0915c6>, 2023.
- 749 Hersbach, H., Bell, B., Berrisford, P., Hirahara, S., Horányi, A., Muñoz-Sabater, J., Nicolas,  
750 J., Peubey, C., Radu, R., Schepers, D., Simmons, A., Soci, C., Abdalla, S., Abellan, X.,  
751 Balsamo, G., Bechtold, P., Biavati, G., Bidlot, J., Bonavita, M., De Chiara, G., Dahlgren, P.,  
752 Dee, D., Diamantakis, M., Dragani, R., Flemming, J., Forbes, R., Fuentes, M., Geer, A.,  
753 Haimberger, L., Healy, S., Hogan, R. J., Hólm, E., Janisková, M., Keeley, S., Laloyaux, P.,  
754 Lopez, P., Lupu, C., Radnoti, G., de Rosnay, P., Rozum, I., Vamborg, F., Villaume, S., and  
755 Thépaut, J.-N.: The ERA5 global reanalysis, *Q. J. R. Meteorol. Soc.*, 146, 1999-2049,  
756 <https://doi.org/10.1002/qj.3803>, 2020.
- 757 Hirsikko, A., Bergman, T., Laakso, L., Dal Maso, M., Riipinen, I., Hörrak, U., and Kulmala,  
758 M.: Identification and classification of the formation of intermediate ions measured in boreal  
759 forest, *Atmos. Chem. Phys.*, 7, 201-210, <https://doi.org/10.5194/acp-7-201-2007>, 2007.
- 760 Hirsikko, A., Vakkari, V., Tiitta, P., Manninen, H. E., Gagné, S., Laakso, H., Kulmala, M.,  
761 Mirme, A., Mirme, S., Mabaso, D., Beukes, J. P., and Laakso, L.: Characterisation of sub-  
762 micron particle number concentrations and formation events in the western Bushveld Igneous  
763 Complex, South Africa, *Atmos. Chem. Phys.*, 12, 3951-3967, [https://doi.org/10.5194/acp-12-](https://doi.org/10.5194/acp-12-3951-2012)  
764 3951-2012, 2012.
- 765 Hooda, R. K., Kivekäs, N., O'Connor, E. J., Collaud Coen, M., Pietikäinen, J.-P., Vakkari, V.,  
766 Backman, J., Henriksson, S. V., Asmi, E., Komppula, M., Korhonen, H., Hyvärinen, A.-P., and  
767 Lihavainen, H.: Driving Factors of Aerosol Properties Over the Foothills of Central Himalayas  
768 Based on 8.5 Years Continuous Measurements, *J. Geophys. Res.*, 123, 13,421-413,442,  
769 <https://doi.org/10.1029/2018jd029744>, 2018.



- 770 Hussein, T., Atashi, N., Sogacheva, L., Hakala, S., Dada, L., Petäjä, T., and Kulmala, M.:  
771 Characterization of Urban New Particle Formation in Amman—Jordan, *Atmosphere*, 11, 79,  
772 <https://doi.org/10.3390/atmos11010079> 2020.
- 773 Hyvärinen, A. P., Lihavainen, H., Komppula, M., Panwar, T. S., Sharma, V. P., Hooda, R. K.,  
774 and Viisanen, Y.: Aerosol measurements at the Gual Pahari EUCAARI station: preliminary  
775 results from in-situ measurements, *Atmos. Chem. Phys.*, 10, 7241-7252,  
776 <https://doi.org/10.5194/acp-10-7241-2010>, 2010.
- 777 IPCC: Climate Change 2023: Synthesis Report. Contribution of Working Groups I, II and III  
778 to the Sixth Assessment Report of the Intergovernmental Panel on Climate Change [Core  
779 Writing Team, H. Lee and J. Romero (eds.)]. IPCC, Geneva, Switzerland, 184 pp.,  
780 <https://doi.org/10.59327/IPCC/AR6-9789291691647>, 2023.
- 781 Jokinen, T., Kontkanen, J., Lehtipalo, K., Manninen, H. E., Aalto, J., Porcar-Castell,  
782 A., Garmash, O., Nieminen, T., Ehn, M., Kangasluoma, J., Junninen, H., Levula, J., Duplissy,  
783 J., Ahonen, L. R., Rantala, P., Heikkinen, L., Yan, C., Sipilä, M., Worsnop, D. R., Bäck, J., a  
784 Petäjä, T., Kerminen, V. M., Kulmala, M.: Solar eclipse demonstrating the importance of  
785 photochemistry in new particle formation. *Scientific Reports*, 7(1), 45707.  
786 <https://doi.org/10.1038/srep45707>, 2017.
- 787 Kalivitis, N., Kerminen, V. M., Kouvarakis, G., Stavroulas, I., Tzitzikalaki, E., Kalkavouras,  
788 P., Daskalakis, N., Myriokefalitakis, S., Bougiatioti, A., Manninen, H. E., Roldin, P., Petäjä,  
789 T., Boy, M., Kulmala, M., Kanakidou, M., and Mihalopoulos, N.: Formation and growth of  
790 atmospheric nanoparticles in the eastern Mediterranean: results from long-term measurements  
791 and process simulations, *Atmos. Chem. Phys.*, 19, 2671-2686, <https://doi.org/10.5194/acp-19-2671-2019>, 2019.
- 793 Kalkavouras, P., Bougiatioti, A., Hussein, T., Kalivitis, N., Stavroulas, I., Michalopoulos, P.,  
794 and Mihalopoulos, N.: Regional New Particle Formation over the Eastern Mediterranean and  
795 Middle East, *Atmosphere*, 12, <https://doi.org/10.3390/atmos12010013>, 2021.
- 796 Kalkavouras, P., Bougiatioti, A., Kalivitis, N., Stavroulas, I., Tombrou, M., Nenes, A., and  
797 Mihalopoulos, N.: Regional new particle formation as modulators of cloud condensation nuclei  
798 and cloud droplet number in the eastern Mediterranean, *Atmos. Chem. Phys.*, 19, 6185-6203,  
799 <https://doi.org/10.5194/acp-19-6185-2019>, 2019.
- 800 Kalkavouras, P., Bougiatioti, A., Grivas, G., Stavroulas, I., Kalivitis, N., Liakakou, E.,  
801 Gerasopoulos, E., Pilinis, C., and Mihalopoulos, N.: On the regional aspects of new particle  
802 formation in the Eastern Mediterranean: A comparative study between a background and an  
803 urban site based on long term observations, *Atmos. Res.*, 239, 104911,  
804 <https://doi.org/10.1016/j.atmosres.2020.104911>, 2020.
- 805 Kanawade, V. and Tripathi, S. N.: Evidence for the role of ion-induced particle formation  
806 during an atmospheric nucleation event observed in Tropospheric Ozone Production about the  
807 Spring Equinox (TOPSE), *J. Geophys. Res.*, 111, D02209,  
808 <https://doi.org/10.1029/2005JD006366>, 2006.
- 809 Kanawade, V. P., Benson, D. R., & Lee, S.-H. . Statistical analysis of 4-year observations of  
810 aerosol sizes in a semi-rural continental environment, *Atmos. Environ.*, 59, 30–38.  
811 <https://doi.org/10.1016/j.atmosenv.2012.05.047>, 2012.



- 812 Kanawade, V. P., Sebastian, M., Hooda, R. K., and Hyvärinen, A. P.: Atmospheric new particle  
813 formation in India: Current understanding, knowledge gaps and future directions, *Atmos.*  
814 *Environ.*, 270, 118894, <https://doi.org/10.1016/j.atmosenv.2021.118894>, 2021.
- 815 Kanawade, V. P., Tripathi, S. N., Siingh, D., Gautam, A. S., Srivastava, A. K., Kamra, A. K.,  
816 Soni, V. K., and Sethi, V.: Observations of new particle formation at two distinct Indian  
817 subcontinental urban locations, *Atmos. Environ.*, 96, 370-379,  
818 <http://dx.doi.org/10.1016/j.atmosenv.2014.08.001>, 2014.
- 819 Kerminen, V. M., Chen, X., Vakkari, V., Petäjä, T., Kulmala, M., and Bianchi, F.: Atmospheric  
820 new particle formation and growth: review of field observations, *Environ. Res. Lett.*, 13,  
821 103003, <https://doi.org/10.1088/1748-9326/aadf3c>, 2018.
- 822 Kerminen, V. M., Paramonov, M., Anttila, T., Riipinen, I., Fountoukis, C., Korhonen, H.,  
823 Asmi, E., Laakso, L., Lihavainen, H., Swietlicki, E., Svenningsson, B., Asmi, A., Pandis, S.  
824 N., Kulmala, M., and Petäjä, T.: Cloud condensation nuclei production associated with  
825 atmospheric nucleation: a synthesis based on existing literature and new results, *Atmos. Chem.*  
826 *Phys.*, 12, 12037-12059, <https://doi.org/10.5194/acp-12-12037-2012>, 2012.
- 827 Kotthaus, S., Bravo-Aranda, J. A., Collaud Coen, M., Guerrero-Rascado, J. L., Costa, M. J.,  
828 Cimini, D., O'Connor, E. J., Hervo, M., Alados-Arboledas, L., Jiménez-Portaz, M., Mona, L.,  
829 Ruffieux, D., Illingworth, A., and Haefelin, M.: Atmospheric boundary layer height from  
830 ground-based remote sensing: a review of capabilities and limitations, *Atmos. Meas. Tech.*, 16,  
831 433-479, <https://doi.org/10.5194/amt-16-433-2023>, 2023.
- 832 Kulmala, M.: How Particles Nucleate and Grow, 302, 1000-1001,  
833 <https://doi.org/10.1126/science.1090848>, 2003.
- 834 Kulmala, M., Vehkamäki, H., Petäjä, T., Dal Maso, M., Lauri, A., Kerminen, V. M., Birmili,  
835 W., and McMurry, P. H.: Formation and growth rates of ultrafine atmospheric particles: a  
836 review of observations, *J. Aerosol Sci.*, 35, 143-176,  
837 <http://dx.doi.org/10.1016/j.jaerosci.2003.10.003>, 2004.
- 838 Kulmala, M., Aliaga, D., Tuovinen, S., Cai, R., Junninen, H., Yan, C., Bianchi, F., Cheng, Y.,  
839 Ding, A., Worsnop, D. R., Petäjä, T., Lehtipalo, K., Paasonen, P., and Kerminen, V. M.:  
840 Opinion: A paradigm shift in investigating the general characteristics of atmospheric new  
841 particle formation using field observations, *Aerosol Research*, 2, 49-58,  
842 <https://doi.org/10.5194/ar-2-49-2024>, 2024.
- 843 Kulmala, M., Petäjä, T., Nieminen, T., Sipilä, M., Manninen, H. E., Lehtipalo, K., Dal Maso,  
844 M., Aalto, P. P., Junninen, H., Paasonen, P., Riipinen, I., Lehtinen, K. E. J., Laaksonen, A., and  
845 Kerminen, V. M.: Measurement of the nucleation of atmospheric aerosol particles, *Nat. Protoc.*,  
846 7, 1651-1667, <https://doi.org/10.1038/nprot.2012.091>, 2012.
- 847 Lee, S.-H., Gordon, H., Yu, H., Lehtipalo, K., Haley, R., Li, Y., and Zhang, R.: New Particle  
848 Formation in the Atmosphere: From Molecular Clusters to Global Climate, *J. Geophys. Res.:*  
849 *Atmos.*, 124, 7098-7146, <https://doi.org/10.1029/2018JD029356>, 2019.
- 850 Lee, S. H., Young, L.-H., Benson, D. R., Suni, T., Kulmala, M., Junninen, H., Campos, T. L.,  
851 Rogers, D. C., and Jensen, J.: Observations of nighttime new particle formation in the  
852 troposphere, *J. Geophys. Res.:* *Atmos.*, 113, <https://doi.org/10.1029/2007JD009351>, 2008.



- 853 Lelieveld, J., Klingmüller, K., Pozzer, A., Burnett, R. T., Haines, A., and Ramanathan, V.:  
854 Effects of fossil fuel and total anthropogenic emission removal on public health and climate,  
855 Proc. Natl. Acad. Sci. 116, 7192-7197, <https://doi.org/10.1073/pnas.1819989116>, 2019.
- 856 Mäkelä, J. M., Riihelä, M., Ukkonen, A., Jokinen, V., and Keskinen, J.: Comparison of  
857 mobility equivalent diameter with Kelvin-Thomson diameter using ion mobility data, J. Chem.  
858 Phys., 105, 1562-1571, <https://doi.org/10.1063/1.472017>, 1996.
- 859 Manninen, H. E., Mirme, S., Mirme, A., Petäjä, T., and Kulmala, M.: How to reliably detect  
860 molecular clusters and nucleation mode particles with Neutral cluster and Air Ion Spectrometer  
861 (NAIS), Atmos. Meas. Tech., 9, 3577-3605, <https://doi.org/10.5194/amt-9-3577-2016>, 2016.
- 862 Manninen, H. E., Nieminen, T., Asmi, E., Gagné, S., Häkkinen, S., Lehtipalo, K., Aalto, P.,  
863 Vana, M., Mirme, A., Mirme, S., Hörrak, U., Plass-Dülmer, C., Stange, G., Kiss, G., Hoffer,  
864 A., Törő, N., Moerman, M., Henzing, B., de Leeuw, G., Brinkenberg, M., Kouvarakis, G. N.,  
865 Bougiatioti, A., Mihalopoulos, N., O'Dowd, C., Ceburnis, D., Arneth, A., Svenningsson, B.,  
866 Swietlicki, E., Tarozzi, L., Decesari, S., Facchini, M. C., Birmili, W., Sonntag, A.,  
867 Wiedensohler, A., Boulon, J., Sellegri, K., Laj, P., Gysel, M., Bukowiecki, N., Weingartner,  
868 E., Wehrle, G., Laaksonen, A., Hamed, A., Joutsensaari, J., Petäjä, T., Kerminen, V.-M., and  
869 Kulmala, M.: EUCAARI ion spectrometer measurements at 12 European sites – analysis of  
870 new particle formation events, Atmos. Chem. Phys., 10, 7907-7927,  
871 <https://doi.org/10.5194/acp-10-7907-2010>, 2010.
- 872 Merikanto, J., Spracklen, D. V., Mann, G. W., Pickering, S. J., and Carslaw, K. S.: Impact of  
873 nucleation on global CCN, Atmos. Chem. Phys., 9, 8601-8616, <https://doi.org/10.5194/acp-9-8601-2009>, 2009.
- 875 Minguillón, M. C., Brines, M., Pérez, N., Reche, C., Pandolfi, M., Fonseca, A. S., Amato, F.,  
876 Alastuey, A., Lyasota, A., Codina, B., Lee, H. K., Eun, H. R., Ahn, K. H., and Querol, X.: New  
877 particle formation at ground level and in the vertical column over the Barcelona area,  
878 Atmospheric Research, 164-165, 118-130, <https://doi.org/10.1016/j.atmosres.2015.05.003>,  
879 2015.
- 880 Mirme, S. and Mirme, A.: The mathematical principles and design of the NAIS – a  
881 spectrometer for the measurement of cluster ion and nanometer aerosol size distributions,  
882 Atmos. Meas. Tech., 6, 1061-1071, <https://doi.org/10.5194/amt-6-1061-2013>, 2013.
- 883 Münkel, C. and Roininen, R.: Automatic monitoring of boundary layer structures with  
884 ceilometers, Bound.-Lay. Meteorol., 124, 117-128, <https://doi.org/10.1007/s10546-006-9103-3>,  
885 2010.
- 886 Nie, W., Ding, A., Wang, T., Kerminen, V.-M., George, C., Xue, L., Wang, W., Zhang, Q.,  
887 Petäjä, T., Qi, X., Gao, X., Wang, X., Yang, X., Fu, C., and Kulmala, M.: Polluted dust  
888 promotes new particle formation and growth, Scientific Reports, 4, 6634,  
889 <https://doi.org/10.1038/srep06634>, 2014.
- 890 Nieminen, T., Asmi, A., Maso, M. D., Aalto, P. P., Keronen, P., Petaja, T., Kulmala, M., and  
891 Kerminen, V.-M.: Trends in atmospheric new-particle formation: 16 years of observations in a  
892 boreal-forest environment, Boreal Environ. Res., 19, 191-214, ISSN 1797-2469, 2014.



- 893 Nieminen, T., Kerminen, V. M., Petäjä, T., Aalto, P. P., Arshinov, M., Asmi, E., Baltensperger,  
894 U., Beddows, D. C. S., Beukes, J. P., Collins, D., Ding, A., Harrison, R. M., Henzing, B.,  
895 Hooda, R., Hu, M., Hörrak, U., Kivekäs, N., Komsaare, K., Krejci, R., Kristensson, A., Laakso,  
896 L., Laaksonen, A., Leaitch, W. R., Lihavainen, H., Mihalopoulos, N., Németh, Z., Nie, W.,  
897 O'Dowd, C., Salma, I., Sellegri, K., Svenningsson, B., Swietlicki, E., Tunved, P., Ulevicius,  
898 V., Vakkari, V., Vana, M., Wiedensohler, A., Wu, Z., Virtanen, A., and Kulmala, M.: Global  
899 analysis of continental boundary layer new particle formation based on long-term  
900 measurements, *Atmos. Chem. Phys.*, 18, 14737-14756, [https://doi.org/10.5194/acp-18-14737-](https://doi.org/10.5194/acp-18-14737-2018)  
901 2018, 2018.
- 902 O'Donnell, S. E., Akherati, A., He, Y., Hodshire, A. L., Shilling, J. E., Kuang, C., Fast, J. D.,  
903 Mei, F., Schobesberger, S., Thornton, J. A., Smith, J. N., Jathar, S. H., and Pierce, J. R.: Look  
904 Up: Probing the Vertical Profile of New Particle Formation and Growth in the Planetary  
905 Boundary Layer With Models and Observations, *J. Geophys. Res.*, 128, e2022JD037525,  
906 <https://doi.org/10.1029/2022JD037525>, 2023.
- 907 Pierce, J. R. and Adams, P. J.: Uncertainty in global CCN concentrations from uncertain  
908 aerosol nucleation and primary emission rates, *Atmos. Chem. Phys.*, 9, 1339-1356,  
909 <https://doi.org/10.5194/acp-9-1339-2009>, 2009.
- 910 Pikridas, M., Riipinen, I., Hildebrandt, L., Kostenidou, E., Manninen, H., Mihalopoulos, N.,  
911 Kalivitis, N., Burkhardt, J. F., Stohl, A., Kulmala, M., and Pandis, S. N.: New particle formation  
912 at a remote site in the eastern Mediterranean, *J. Geophys. Res.*, 117,  
913 <https://doi.org/10.1029/2012JD017570>, 2012.
- 914 Platis, A., Altstädter, B., Wehner, B., Wildmann, N., Lampert, A., Hermann, M., Birmili, W.,  
915 and Bange, J.: An Observational Case Study on the Influence of Atmospheric Boundary-Layer  
916 Dynamics on New Particle Formation, *Boundary-Layer Meteorology*, 158, 67-92,  
917 <https://doi.org/10.1007/s10546-015-0084-y>, 2016.
- 918 Rose, C., Sellegri, K., Freney, E., Dupuy, R., Colomb, A., Pichon, J. M., Ribeiro, M.,  
919 Bourianne, T., Burnet, F., and Schwarzenboeck, A.: Airborne measurements of new particle  
920 formation in the free troposphere above the Mediterranean Sea during the HYMEX campaign,  
921 *Atmos. Chem. Phys.*, 15, 10203-10218, <https://doi.org/10.5194/acp-15-10203-2015>, 2015.
- 922 Schröder, F. and Ström, J.: Aircraft measurements of sub micrometer aerosol particles ( $> 7$   
923 nm) in the midlatitude free troposphere and tropopause region, *Atmospheric Research*, 44, 333-  
924 356, [https://doi.org/10.1016/S0169-8095\(96\)00034-8](https://doi.org/10.1016/S0169-8095(96)00034-8), 1997.
- 925 Sebastian, M., Kanawade, V. P., Soni, V., Asmi, E., Westervelt, D. M., Vakkari, V., Hyvärinen,  
926 A. P., Pierce, J. R., and Hooda, R. K.: New Particle Formation and Growth to Climate-Relevant  
927 Aerosols at a Background Remote Site in the Western Himalaya, *J. Geophys. Res.*, 126,  
928 e2020JD033267, <https://doi.org/10.1029/2020JD033267>, 2021.
- 929 Sebastian, M., Kompalli, S. K., Kumar, V. A., Jose, S., Babu, S. S., Pandithurai, G., Singh, S.,  
930 Hooda, R. K., Soni, V. K., Pierce, J. R., Vakkari, V., Asmi, E., Westervelt, D. M., Hyvärinen,  
931 A. P., and Kanawade, V. P.: Observations of particle number size distributions and new particle  
932 formation in six Indian locations, *Atmos. Chem. Phys.*, 22, 4491-4508,  
933 <https://doi.org/10.5194/acp-22-4491-2022>, 2022.





- 934 Sellegri, K., Rose, C., Marinoni, A., Lupi, A., Wiedensohler, A., Andrade, M., Bonasoni, P.,  
935 and Laj, P.: New Particle Formation: A Review of Ground-Based Observations at Mountain  
936 Research Stations, *Atmosphere*, 10, 493, <https://doi.org/10.3390/atmos10090493>, 2019.
- 937 Spracklen, D. V., Carslaw, K. S., Kulmala, M., Kerminen, V.-M., Sihto, S.-L., Riipinen, I.,  
938 Merikanto, J., Mann, G. W., Chipperfield, M. P., Wiedensohler, A., Birmili, W., and  
939 Lihavainen, H.: Contribution of particle formation to global cloud condensation nuclei  
940 concentrations, *Geophys. Res. Lett.*, 35, 2007GL033038,  
941 <https://doi.org/10.1029/2007gl033038>, 2008.
- 942 Stratmann, F., Siebert, H., Spindler, G., Wehner, B., Althausen, D., Heintzenberg, J., Hellmuth,  
943 O., Rinke, R., Schmieder, U., Seidel, C., Tuch, T., Uhrner, U., Wiedensohler, A., Wandinger,  
944 U., Wendisch, M., Schell, D., and Stohl, A.: New-particle formation events in a continental  
945 boundary layer: first results from the SATURN experiment, *Atmos. Chem. Phys.*, 3, 1445-  
946 1459, <https://doi.org/10.5194/acp-3-1445-2003>, 2003.
- 947 Stull, R. B.: An Introduction to Boundary Layer Meteorology, Atmospheric and  
948 Oceanographic Sciences Library, Springer Dordrecht, <https://doi.org/10.1007/978-94-009-3027-8>, 1988.
- 950 Tröstl, J., Herrmann, E., Frege, C., Bianchi, F., Molteni, U., Bukowiecki, N., Hoyle, C. R.,  
951 Steinbacher, M., Weingartner, E., Dommen, J., Gysel, M., and Baltensperger, U.: Contribution  
952 of new particle formation to the total aerosol concentration at the high-altitude site  
953 Jungfraujoch (3580 m asl, Switzerland), *J. Geophys. Res.*, 121, 11,692-611,711,  
954 <https://doi.org/10.1002/2015jd024637>, 2016a.
- 955 Tröstl, J., Chuang, W. K., Gordon, H., Heinritzi, M., Yan, C., Molteni, U., Ahlm, L., Frege, C.,  
956 Bianchi, F., Wagner, R., Simon, M., Lehtipalo, K., Williamson, C. J., Craven, J. S., Duplissy,  
957 J., Adamov, A., Almeida, J., Bernhammer, A. K., Breitenlechner, M., Brilke, S., Dias, A.,  
958 Ehrhart, S., Flagan, R. C., Franchin, A., Fuchs, C., Guida, R., Gysel, M., Hansel, A., Hoyle, C.  
959 R., Jokinen, T., Junninen, H., Kangasluoma, J., Keskinen, H., Kim, J., Krapf, M., Kürten, A.,  
960 Laaksonen, A., Lawler, M. J., Leiminger, M., Mathot, S., Möhler, O., Nieminen, T., Onnela,  
961 A., Petäjä, T., Piel, F. M., Miettinen, P., Rissanen, M. P., Rondo, L., Sarnela, N.,  
962 Schobesberger, S., Sengupta, K., Sipilä, M., Smith, J. N., Steiner, G., Tomè, A., Virtanen, A.,  
963 Wagner, A. C., Weingartner, E., Wimmer, D., Winkler, P. M., Ye, P., Carslaw, K. S., Curtius,  
964 J., Dommen, J., Kirkby, J., Kulmala, M., Riipinen, I., Worsnop, D. R., Donahue, N. M., and  
965 Baltensperger, U.: The role of low-volatility organic compounds in initial particle growth in  
966 the atmosphere, *Nature*, 533, 527-531, <https://doi.org/10.1038/nature18271>, 2016b.
- 967 Vrekoussis, M., Pikridas, M., Rousogenous, C., Christodoulou, A., Desservettaz, M., Sciare,  
968 J., Richter, A., Bougoudis, I., Savvides, C., and Papadopoulos, C.: Local and regional air  
969 pollution characteristics in Cyprus: A long-term trace gases observations analysis, *Sci. Total  
970 Environ.*, 845, 157315, <https://doi.org/10.1016/j.scitotenv.2022.157315>, 2022.
- 971 Wang, M. and Penner, J. E.: Aerosol indirect forcing in a global model with particle nucleation,  
972 *Atmos. Chem. Phys.*, 9, 239-260, <https://doi.org/10.5194/acp-9-239-2009>, 2009.
- 973 Wehner, B., Werner, F., Ditas, F., Shaw, R. A., Kulmala, M., and Siebert, H.: Observations of  
974 new particle formation in enhanced UV irradiance zones near cumulus clouds, *Atmos. Chem.  
975 Phys.*, 15, 11701-11711, <https://doi.org/10.5194/acp-15-11701-2015>, 2015.



- 976 Wehner, B., Siebert, H., Ansmann, A., Ditas, F., Seifert, P., Stratmann, F., Wiedensohler, A.,  
977 Apituley, A., Shaw, R. A., Manninen, H. E., and Kulmala, M.: Observations of turbulence-  
978 induced new particle formation in the residual layer, *Atmos. Chem. Phys.*, 10, 4319-4330,  
979 <https://doi.org/10.5194/acp-10-4319-2010>, 2010.
- 980 Westervelt, D. M., Pierce, J. R., and Adams, P. J.: Analysis of feedbacks between nucleation  
981 rate, survival probability and cloud condensation nuclei formation, *Atmos. Chem. Phys.*, 14,  
982 5577-5597, <https://doi.org/10.5194/acp-14-5577-2014>, 2014.
- 983 Westervelt, D. M., Pierce, J. R., Riipinen, I., Trivitanurak, W., Hamed, A., Kulmala, M.,  
984 Laaksonen, A., Decesari, S., and Adams, P. J.: Formation and growth of nucleated particles  
985 into cloud condensation nuclei: model-measurement comparison, *Atmos. Chem. Phys.*, 13,  
986 7645-7663, <https://doi.org/10.5194/acp-13-7645-2013>, 2013.
- 987 Williamson, C. J., Kupc, A., Axisa, D., Bilsback, K. R., Bui, T., Campuzano-Jost, P., Dollner,  
988 M., Froyd, K. D., Hodshire, A. L., Jimenez, J. L., Kodros, J. K., Luo, G., Murphy, D. M., Nault,  
989 B. A., Ray, E. A., Weinzierl, B., Wilson, J. C., Yu, F., Yu, P., Pierce, J. R., and Brock, C. A.:  
990 A large source of cloud condensation nuclei from new particle formation in the tropics, *Nature*,  
991 574, 399-403, <https://doi.org/10.1038/s41586-019-1638-9>, 2019.
- 992 Wu, Z., Hu, M., Liu, S., Wehner, B., Bauer, S., Maßling, A., Wiedensohler, A., Petäjä, T., Dal  
993 Maso, M., Kulmala, M.: New particle formation in Beijing, China: Statistical analysis of a 1-  
994 year data set, *J. Geophys. Res.*, 112, D09209, <https://doi.org/10.1029/2006JD007406>, 2007.
- 995 Yu, F. and Luo, G.: Simulation of particle size distribution with a global aerosol model:  
996 contribution of nucleation to aerosol and CCN number concentrations, *Atmos. Chem. Phys.*, 9,  
997 7691-7710, <https://doi.org/10.5194/acp-9-7691-2009>, 2009.
- 998 Zha, Q., Aliaga, D., Krejci, R., Sinclair, V. A., Wu, C., Ciarelli, G., Scholz, W., Heikkinen, L.,  
999 Partoll, E., Gramlich, Y., Huang, W., Leiminger, M., Enroth, J., Peräkylä, O., Cai, R., Chen,  
1000 X., Koenig, A. M., Velarde, F., Moreno, I., Petäjä, T., Artaxo, P., Laj, P., Hansel, A., Carbone,  
1001 S., Kulmala, M., Andrade, M., Worsnop, D., Mohr, C., and Bianchi, F.: Oxidized organic  
1002 molecules in the tropical free troposphere over Amazonia, *National Science Review*, 11,  
1003 <https://doi.org/10.1093/nsr/nwad138>, 2023.
- 1004 Zhang, D., Comstock, J., and Morris, V.: Comparison of planetary boundary layer height from  
1005 ceilometer with ARM radiosonde data, *Atmos. Meas. Tech.*, 15, 4735-4749,  
1006 <https://doi.org/10.5194/amt-15-4735-2022>, 2022.
- 1007 Zhang, R., Suh, I., Zhao, J., Zhang, D., Fortner, E. C., Tie, X., Molina, L. T., and Molina, M.  
1008 J.: Atmospheric New Particle Formation Enhanced by Organic Acids, *Science*, 304, 1487-  
1009 1490, <https://doi.org/10.1126/science.1095139>, 2004.
- 1010 Zhao, B., Shrivastava, M., Donahue, N. M., Gordon, H., Schervish, M., Shilling, J. E., Zaveri,  
1011 R. A., Wang, J., Andreae, M. O., Zhao, C., Gaudet, B., Liu, Y., Fan, J., and Fast, J. D.: High  
1012 concentration of ultrafine particles in the Amazon free troposphere produced by organic new  
1013 particle formation, *Proc. Natl. Acad. Sci.*, 117, 25344-25351,  
1014 <https://doi.org/10.1073/pnas.2006716117>, 2020.
- 1015 Zittis, G., Almazroui, M., Alpert, P., Ciais, P., Cramer, W., Dahdal, Y., Fnais, M., Francis, D.,  
1016 Hadjinicolaou, P., Howari, F., Jrrar, A., Kaskaoutis, D. G., Kulmala, M., Lazoglou, G.,



1017 Mihalopoulos, N., Lin, X., Rudich, Y., Sciare, J., Stenchikov, G., Xoplaki, E., and Lelieveld,  
1018 J.: Climate Change and Weather Extremes in the Eastern Mediterranean and Middle East, Rev.  
1019 Geophys., 60, e2021RG000762, <https://doi.org/10.1029/2021R, G000762>, 2022.

1020

1021